
Supplementary Document

Anonymous Author(s)

Affiliation
Address
email

1 1 Pseudo-code

2 The pseudo-code of plugging our method into the vanilla BO is summarised in Algorithm 1. It is
3 clear to see that the modifications are so minor that the corresponding BO algorithmic framework is
4 kept intact. Therefore, our method is applicable to any other variants of BO in a plug-in manner.

Algorithm 1: BO with the proposed termination criterion

Input: N_I , FE , N , η_{lb}

Data: Sampled initial solutions $\mathcal{X} \leftarrow \{\mathbf{x}^i\}_{i=1}^{N_I}$ from Ω , evaluated objective function values
 $\mathcal{Y} \leftarrow \{f(\mathbf{x}^i)\}_{i=1}^{N_I}$, training data set $\mathcal{D} \leftarrow \{(\mathbf{x}^i, f(\mathbf{x}^i))\}_{i=1}^{N_I}$

Output: \mathcal{D}

Sample N recently observed points in \mathcal{D} and store them in a temporary archive $\tilde{\mathcal{D}}$;
for $t = N_I + 1$ **to** FE **do**

 Train the GP model based on \mathcal{D} ;

 Optimize an acquisition function to obtain the candidate solution \mathbf{x}^t ;

 Update $\tilde{\Omega}$ based on $\tilde{\mathcal{D}}$;

if Condition 1 is met **then**

if Condition 2 is met **then**

 Terminate BO loop;

return \mathcal{D} ;

 Evaluate the objective function value $f(\mathbf{x}^t)$ and update $\mathcal{D} \leftarrow \mathcal{D} \cup \{(\mathbf{x}^t, f(\mathbf{x}^t))\}$;

 Update $\tilde{\mathcal{D}}$;

end

return \mathcal{D} ;

6 2 Proofs of the Theoretical Results in Section 2

7 In this section, we present the proofs associated with the theoretical assertions from Section 2. To
8 ensure the material is self-contained and to aid reader comprehension, we replicate the corresponding
9 theoretical statements here.

10 **Proposition 1.** Consider $\forall \mathbf{x} \in \tilde{\Omega}$, where $-\mu(\mathbf{x})$ represents a convex function. If $\|\nabla \mu(\mathbf{x})\|_2 \leq \lambda$,
11 we can establish:

$$\mu(\dot{\mathbf{x}}) - \mu(\mathbf{x}) \leq \xi, \quad (1)$$

12 where $\lambda = (2m_1\xi)^{1/2}$, ξ is a positive constant, and m_1 denotes the strong convexity parameter of
13 $-\mu(\mathbf{x})$ [1].

¹⁴ *Proof.* Given that $-\mu(\mathbf{x})$ is a convex function with a strong convexity parameter m_1 , by denoting
¹⁵ $-\mu(\mathbf{x})$ as $H(\mathbf{x})$, we apply the second-order Taylor expansion upon $H(\mathbf{x})$:

$$H(\mathbf{x}^1) = H(\mathbf{x}^2) + \nabla H(\mathbf{x}^2)^\top (\mathbf{x}^1 - \mathbf{x}^2) + \frac{1}{2} (\mathbf{x}^1 - \mathbf{x}^2)^\top \nabla^2 H(\mathbf{x}^3) (\mathbf{x}^1 - \mathbf{x}^2), \quad (2)$$

¹⁶ where $\mathbf{x}^1, \mathbf{x}^2 \in \tilde{\Omega}$, and $\mathbf{x}^3 = \alpha \mathbf{x}^1 + (1 - \alpha) \mathbf{x}^2$, $\alpha \in [0, 1]$. Since $\nabla^2 H(\mathbf{x}) \succeq m_1 \mathbf{I}^1$, where \mathbf{I} is an
¹⁷ identity diagonal matrix, we have

$$H(\mathbf{x}^1) \geq H(\mathbf{x}^2) + \nabla H(\mathbf{x}^2)^\top (\mathbf{x}^1 - \mathbf{x}^2) + \frac{m_1}{2} \|\mathbf{x}^1 - \mathbf{x}^2\|_2^2, \quad (3)$$

¹⁸ where $\mathbf{x}^1, \mathbf{x}^2 \in \tilde{\Omega}$. Let $\hat{\mathbf{x}}^1 = \mathbf{x}^2 - \frac{1}{m_1} \nabla H(\mathbf{x}^2) = \underset{\mathbf{x}^1 \in \tilde{\Omega}}{\operatorname{argmin}} H(\mathbf{x}^2) + \nabla H(\mathbf{x}^2)^\top (\mathbf{x}^1 - \mathbf{x}^2) + \frac{m_1}{2} \|\mathbf{x}^1 - \mathbf{x}^2\|_2^2$, we have

$$\begin{aligned} H(\mathbf{x}^1) &\geq H(\mathbf{x}^2) + \nabla H(\mathbf{x}^2)^\top (\mathbf{x}^1 - \mathbf{x}^2) + \frac{m_1}{2} \|\mathbf{x}^1 - \mathbf{x}^2\|_2^2 \\ &\geq H(\mathbf{x}^2) + \nabla H(\mathbf{x}^2)^\top (\hat{\mathbf{x}}^1 - \mathbf{x}^2) + \frac{m_1}{2} \|\hat{\mathbf{x}}^1 - \mathbf{x}^2\|_2^2 \\ &= H(\mathbf{x}^2) - \frac{1}{2m_1} \|\nabla H(\mathbf{x}^2)\|_2^2, \end{aligned} \quad (4)$$

²⁰ where $\mathbf{x}^1, \mathbf{x}^2 \in \tilde{\Omega}$. Thereafter, we have

$$H(\mathbf{x}) - H(\hat{\mathbf{x}}) \leq \frac{1}{2m_1} \|\nabla H(\mathbf{x})\|_2^2, \quad (5)$$

²¹ where $\hat{\mathbf{x}} = \underset{\mathbf{x} \in \tilde{\Omega}}{\operatorname{argmax}} \mu(\mathbf{x})$. By replacing $H(\mathbf{x})$ with $-\mu(\mathbf{x})$, we have

$$\mu(\hat{\mathbf{x}}) - \mu(\mathbf{x}) \leq \frac{1}{2m_1} \|\nabla \mu(\mathbf{x})\|_2^2. \quad (6)$$

²² Given $\|\nabla \mu(\mathbf{x})\|_2 \leq \lambda = (2m_1 \xi)^{1/2}$, we have

$$\mu(\hat{\mathbf{x}}) - \mu(\mathbf{x}) \leq \xi. \quad (7)$$

²³ \square

²⁴ **Lemma 1.** Assume the GP employs a stationary kernel $k(\cdot, \cdot)$. For $\forall \mathbf{x} \in \tilde{\Omega}$, the lower bound of
²⁵ $\sigma^2(\mathbf{x})$ is given by:

$$\underline{\sigma}^2(\mathbf{x}) = k(\mathbf{x}, \mathbf{x}) + c \sum_{i=1}^{|\mathcal{D}|} k^2(\mathbf{x}, \mathbf{x}^i), \quad (8)$$

²⁶ where $c < 0$ is a constant and $\mathbf{x}^i \in \mathcal{D}$ for $i \in \{1, \dots, |\mathcal{D}|\}$.

²⁷ *Proof.* Given an input vector $\mathbf{x} \in \tilde{\Omega}$, the variance of $f(\mathbf{x})$ is predicted as:

$$\sigma^2(\mathbf{x}) = k(\mathbf{x}, \mathbf{x}) - \mathbf{k}^{*\top} (K + \sigma_\epsilon^2 I)^{-1} \mathbf{k}^*, \quad (9)$$

²⁸ where $X = (\mathbf{x}^1, \dots, \mathbf{x}^N)^\top$, $N = |\mathcal{D}|$. \mathbf{k}^* is the covariance vector between X and \mathbf{x} , and K is the
²⁹ covariance matrix of X . By applying the Cholesky Factorization on K , we rewrite equation (9) as:

$$\sigma^2(\mathbf{x}) = k(\mathbf{x}, \mathbf{x}) - (L^{-1} \mathbf{k}^*)^\top L^{-1} \mathbf{k}^*, \quad (10)$$

³⁰ where $LL^\top = K + \sigma_\epsilon^2 I$. Let us denote

$$L^{-1} = \begin{bmatrix} l_{11} & \cdots & 0 \\ \vdots & \ddots & \vdots \\ l_{1N} & \cdots & l_{NN} \end{bmatrix}, \quad (11)$$

³¹ then we have

$$L^{-1} \mathbf{k}^* = \begin{bmatrix} l_{11} k(\mathbf{x}, \mathbf{x}^1) \\ \vdots \\ \sum_{i=1}^N l_{iN} k(\mathbf{x}, \mathbf{x}^i) \end{bmatrix}. \quad (12)$$

¹ \succeq means that the eigenvalues of $\nabla^2 H(\mathbf{x})$ are greater than m_1 .

32 By introducing equation (12) into equation (10), we have

$$\sigma^2(\mathbf{x}) = k(\mathbf{x}, \mathbf{x}) - \left((l_{11}k(\mathbf{x}, \mathbf{x}^1))^2 + \cdots + \left(\sum_{i=1}^N l_{iN}k(\mathbf{x}, \mathbf{x}^i) \right)^2 \right), \quad (13)$$

33 By applying the Cauchy Schwarz's inequalities, we have:

$$\sigma^2(\mathbf{x}) \geq k(\mathbf{x}, \mathbf{x}) - \left(l_{11}^2 k^2(\mathbf{x}, \mathbf{x}^1) + \cdots + \left(\sum_{i=1}^N l_{iN}^2 \right) \left(\sum_{i=1}^N k^2(\mathbf{x}, \mathbf{x}^i) \right) \right), \quad (14)$$

34 Let c be a negative constant and $c \leq -N \max\{l_{11}^2, \dots, \sum_{i=1}^N l_{iN}^2\}$, we have:

$$\underline{\sigma}^2(\mathbf{x}) = k(\mathbf{x}, \mathbf{x}) + c \sum_{i=1}^N k^2(\mathbf{x}, \mathbf{x}^i) \leq \sigma^2(\mathbf{x}). \quad (15)$$

35 \square

36 **Lemma 2.** Given Lemma 1, determining $\operatorname{argmax}_{\mathbf{x} \in \tilde{\Omega}} \underline{\sigma}^2(\mathbf{x})$ is equivalent to solving the following bilevel
37 optimization problem:

$$\begin{aligned} & \underset{\mathbf{x} \in \tilde{\Omega}}{\text{minimize}} \quad d(\mathbf{x}, \mathbf{x}^1, \mathbf{x}^2) = \|\mathbf{x} - \mathbf{x}^1\|_2^2 + \|\mathbf{x} - \mathbf{x}^2\|_2^2 \\ & \text{subject to} \quad \{\mathbf{x}^1, \mathbf{x}^2\} = \operatorname{argmax}_{\substack{\mathbf{x}^1, \mathbf{x}^2 \in \mathcal{D} \cap \tilde{\Omega} \\ \mathbf{x}^1 \neq \mathbf{x}^2, \tilde{\Omega} \cap \mathcal{D} = \emptyset}} \|\mathbf{x}^1 - \mathbf{x}^2\|_2^2, \end{aligned} \quad (16)$$

38 where $\hat{\Omega} = [\hat{x}_i^L, \hat{x}_i^U]_{i=1}^n \subset \tilde{\Omega}$, $\hat{x}_i^L = \min(x_i^1, x_i^2)$ and $\hat{x}_i^U = \max(x_i^1, x_i^2)$. Given that the lower-level
39 optimization can be addressed via exhaustive search, the analytical solution of (19) is given by
40 $\hat{\mathbf{x}} = (\hat{x}_1^L + \frac{\hat{x}_1^U - \hat{x}_1^L}{2}, \dots, \hat{x}_n^L + \frac{\hat{x}_n^U - \hat{x}_n^L}{2})^\top$.

41 *Proof.* Given a stationary and isotropic kernel $k(\cdot, \cdot)$, we have

$$k^2(\mathbf{x}, \mathbf{x}^i) \propto -\|\mathbf{x} - \mathbf{x}^i\|_2^2, \quad (17)$$

42 where $\mathbf{x} \in \tilde{\Omega}$ and $\mathbf{x}^i \in \mathcal{D}$. Therefore, we can find the $\hat{\Omega}$ that contain $\operatorname{argmax}_{\mathbf{x} \in \tilde{\Omega}} \underline{\sigma}^2(\mathbf{x})$ by solving the
43 following optimization problem:

$$\begin{aligned} \{\mathbf{x}^1, \mathbf{x}^2\} &= \underset{\mathbf{x}^1 \in \mathcal{D} \cap \tilde{\Omega}, \mathbf{x}^2 \in \mathcal{D} \cap \tilde{\Omega}}{\text{maximize}} \|\mathbf{x}^1 - \mathbf{x}^2\|_2^2 \\ &\text{subject to} \quad \mathbf{x}^1 \neq \mathbf{x}^2, \hat{\Omega} \cap \mathcal{D} = \emptyset. \end{aligned} \quad (18)$$

44 Since $\mathcal{D} \cap \tilde{\Omega}$ consists of limited elements, we can find the exact solution of (18) by exhaustive search.

45 Since $\hat{\Omega} \cap \mathcal{D} = \emptyset$ and $k(\cdot, \cdot)$ is isotropic, determining $\operatorname{minimize}_{\mathbf{x} \in \tilde{\Omega}} d(\mathbf{x}, \mathbf{x}^1, \mathbf{x}^2) = \|\mathbf{x} - \mathbf{x}^1\|_2^2 + \|\mathbf{x} - \mathbf{x}^2\|_2^2$

46 is equivalent to solving $\operatorname{maximize}_{\mathbf{x} \in \hat{\Omega}} \underline{\sigma}^2(\mathbf{x})$. To sum up, we can find the exact solution of $\operatorname{argmax}_{\mathbf{x} \in \tilde{\Omega}} \underline{\sigma}^2(\mathbf{x})$
47 by solving the following bi-level optimization problem:

$$\begin{aligned} & \underset{\mathbf{x} \in \tilde{\Omega}}{\text{minimize}} \quad d(\mathbf{x}, \mathbf{x}^1, \mathbf{x}^2) = \|\mathbf{x} - \mathbf{x}^1\|_2^2 + \|\mathbf{x} - \mathbf{x}^2\|_2^2 \\ & \text{subject to} \quad \{\mathbf{x}^1, \mathbf{x}^2\} = \operatorname{argmax}_{\substack{\mathbf{x}^1, \mathbf{x}^2 \in \mathcal{D} \cap \tilde{\Omega} \\ \mathbf{x}^1 \neq \mathbf{x}^2, \hat{\Omega} \cap \mathcal{D} = \emptyset}} \|\mathbf{x}^1 - \mathbf{x}^2\|_2^2, \end{aligned} \quad (19)$$

48 where $\operatorname{argmin}_{\mathbf{x} \in \tilde{\Omega}} d(\mathbf{x}, \mathbf{x}^1, \mathbf{x}^2)$ has an analytical solution $\hat{\mathbf{x}} = (\hat{x}_1^L + \frac{\hat{x}_1^U - \hat{x}_1^L}{2}, \dots, \hat{x}_n^L + \frac{\hat{x}_n^U - \hat{x}_n^L}{2})^\top$. \square

49 **Proposition 2.** Leveraging Lemma 2, suppose $\operatorname{minimize}_{\mathbf{x} \in \tilde{\Omega}} -\sigma^2(\mathbf{x})$ exhibits convexity in its local
50 optimal regions, the following inequality is satisfied when $\|\nabla \sigma^2(\mathbf{x})\|_2 \leq \lambda$:

$$\sigma^2(\hat{\mathbf{x}}) - \sigma^2(\mathbf{x}) \leq \beta + \xi, \quad (20)$$

51 where $\lambda = (2m_2\xi)^{1/2}$, $\xi > 0$, $m_2 > 0$ represents the strong convexity parameter of $-\sigma^2(\mathbf{x})$ in its
52 local optimal regions [1], and β is constrained by $0 \leq \beta \leq \sigma^2(\hat{\mathbf{x}}) - \sigma^2(\hat{\mathbf{x}})$.

53 *Proof.* By applying $\hat{\mathbf{x}}$ as the initialization point for $\underset{\mathbf{x} \in \Omega}{\text{maximize}} \sigma^2(\mathbf{x})$, we have:

$$\beta = \sigma^2(\ddot{\mathbf{x}}) - \sigma^2(\hat{\mathbf{x}}) \geq \sigma^2(\ddot{\mathbf{x}}) - \sigma^2(\bar{\mathbf{x}}), \quad (21)$$

54 where $\bar{\mathbf{x}}, \hat{\mathbf{x}} \in \bar{\Omega} \subseteq \tilde{\Omega}$, $\bar{\mathbf{x}}$ is a local optimal solution and $\bar{\Omega}$ is a local optimal region of $\underset{\mathbf{x} \in \Omega}{\text{maximize}} \sigma^2(\mathbf{x})$.

55 Since $\underset{\mathbf{x} \in \tilde{\Omega}}{\text{minimize}} -\sigma^2(\mathbf{x})$ exhibits convexity in its local optimal regions, given Proposition 1 and
56 $\|\nabla \sigma^2(\mathbf{x})\|_2 \leq \lambda$, we have

$$\sigma^2(\bar{\mathbf{x}}) - \sigma^2(\mathbf{x}) \leq \xi, \quad (22)$$

57 where $\mathbf{x} \in \bar{\Omega}$. By introducing equation (22) in to equation (21), we have

$$\sigma^2(\ddot{\mathbf{x}}) - \sigma^2(\mathbf{x}) \leq \beta + \xi. \quad (23)$$

58 \square

59 **Lemma 3.** As per Srinivas et al., the optimization process in BO can be conceptualized as a sampling
60 process from a GP. Hence, for any $\mathbf{x} \in \Omega$, we have:

$$\Pr(|f(\mathbf{x}) - \mu(\mathbf{x})| \leq \omega\sigma(\mathbf{x})) > \delta, \quad (24)$$

61 where $\delta > 0$ signifies the confidence level adhered to by the UCB.

62 *Proof.* This lemma is directly from Srinivas et al.. The proof can be found therein. \square

63 **Corollary 1.** Based on Lemma 3 and Condition 2, we deduce that:

$$\Pr(f^{\text{acq}}(\tilde{\mathbf{x}}^*) + \varepsilon \geq f(\mathbf{x}^*)) > \delta, \quad (25)$$

64 where $\tilde{\mathbf{x}}^* = \underset{\mathbf{x} \in \Omega}{\text{argmax}} f^{\text{acq}}(\mathbf{x})$, and \mathbf{x}^* represents the true global optimum. Furthermore,

$$0 \leq \varepsilon \leq \mu(\dot{\mathbf{x}}) + \omega\sigma(\ddot{\mathbf{x}}) - f^{\text{acq}}(\tilde{\mathbf{x}}^*), \quad (26)$$

65 where $\dot{\mathbf{x}}$, $\ddot{\mathbf{x}}$, and $\tilde{\mathbf{x}}^*$ are elements of $\tilde{\Omega}$, while $\delta > 0$ denotes the confidence level of the UCB.

66 *Proof.* Given Lemma 3, we have $\Pr(\mu(\mathbf{x}) + \omega\sigma(\mathbf{x}) \geq f(\mathbf{x})) > \delta$. Then, let $f^{\text{acq}}(\mathbf{x}) = \mu(\mathbf{x}) + \omega\sigma(\mathbf{x})$
67 and $\tilde{\mathbf{x}}^* = \underset{\mathbf{x} \in \Omega}{\text{argmax}} f^{\text{acq}}(\mathbf{x})$, we have

$$\Pr(f^{\text{acq}}(\tilde{\mathbf{x}}^*) \geq f^{\text{acq}}(\mathbf{x}^*) \geq f(\mathbf{x}^*)) > \delta, \quad (27)$$

68 where $\mathbf{x}^* = \underset{\mathbf{x} \in \Omega}{\text{argmax}} f(\mathbf{x})$. In practice, there exist numeric errors between $\underset{\mathbf{x} \in \Omega}{\text{sup}} f^{\text{acq}}(\mathbf{x})$ and $f^{\text{acq}}(\tilde{\mathbf{x}}^*)$.
69 By denoting the upper bound of the errors as ε , we have

$$\Pr(f^{\text{acq}}(\tilde{\mathbf{x}}^*) + \varepsilon \geq f(\mathbf{x}^*)) > \delta. \quad (28)$$

70 Since $\dot{\mathbf{x}} = \underset{\mathbf{x} \in \tilde{\Omega}}{\text{argmax}} \mu(\mathbf{x})$ and $\ddot{\mathbf{x}} = \underset{\mathbf{x} \in \tilde{\Omega}}{\text{argmax}} \sigma^2(\mathbf{x})$, f^{acq} has the following upper bound:

$$\underset{\mathbf{x} \in \tilde{\Omega}}{\text{sup}} f^{\text{acq}}(\mathbf{x}) \leq \mu(\dot{\mathbf{x}}) + \sigma(\ddot{\mathbf{x}}). \quad (29)$$

71 Therefore, the ε is bounded by

$$0 \leq \varepsilon \leq \mu(\dot{\mathbf{x}}) + \omega\sigma(\ddot{\mathbf{x}}) - f^{\text{acq}}(\tilde{\mathbf{x}}^*), \quad (30)$$

72 where $\dot{\mathbf{x}}, \ddot{\mathbf{x}}, \tilde{\mathbf{x}}^* \in \tilde{\Omega}$. \square

73 **Theorem 1.** Leveraging Corollary 1, when employing the termination method proposed in this paper,
74 we deduce that the global regret bound of BO as:

$$\Pr(r \leq 2\omega\sigma(\tilde{\mathbf{x}}^*) + \varepsilon) > \delta, \quad (31)$$

75 where $\delta > 0$ signifies the confidence level associated with the UCB.

76 *Proof.* We formulate the regret of BO as follows:

$$r = f(\mathbf{x}^*) - \mu(\mathbf{x}) + \mu(\mathbf{x}) - f(\tilde{\mathbf{x}}^*). \quad (32)$$

77 Based on Lemma 3 and Corollary 1, by introducing equation (24) and equation (25) into equation (32),
78 we have

$$\Pr(r \leq 2\omega\sigma(\tilde{\mathbf{x}}^*) + \varepsilon) > \delta. \quad (33)$$

79 \square

80 **Theorem 2.** *Building upon Condition 1 and Condition 2, and employing the termination method
81 proposed in this paper, we establish the local regret bound of BO as:*

$$\Pr(f(\mathbf{x}^*) - f(\mathbf{x}) \leq \tilde{r}) > \delta, \quad (34)$$

82 where $\mathbf{x} \in \tilde{\Omega}$, \mathbf{x}^* denotes the true global optimum in $\tilde{\Omega}$, and $\delta > 0$ is the confidence level of the UCB.
83

84 *Proof.* Based on Theorem 1, by introducing equation (30) into equation (33), we have

$$\Pr(f(\mathbf{x}^*) - f(\mathbf{x}) \leq \tilde{r}) > \delta, \quad (35)$$

85 where $\tilde{r} = \mu(\dot{\mathbf{x}}) - \mu(\tilde{\mathbf{x}}) + \omega(\sigma(\ddot{\mathbf{x}}) + \sigma(\tilde{\mathbf{x}}))$. \square

86 3 Experimental Results

87 3.1 Compelmentary Results

88 In this subsection, we provide the complete experimental results, offering supplementary findings to
89 those presented in the main manuscript. More specifically,

- 90 • Figures Figure 1 to Figure 16 presents the complete results of the trajectories of I_{cdf} collected
91 on all comparisons.
- 92 • Figures 17 to 28 show the complete results of the trajectories of different termination
93 indicators versus the number of FEs during the BO process collected on all comparisons.
- 94 • Figures 29 to 47 provide the complete results of the trajectories of the regret of BO versus
95 the number of FEs during the BO process collected on all comparisons.

96 To ensure the material is self-contained and to aid reader comprehension, we replicate the correspond-
97 ing statements of the three types of benchmark problems here.

- 98 • Synthetic functions: We consider Ackley, Levy, and Schwefel functions [6] with $n \in$
99 $\{2, 5, 10\}$. The objective function $f(\mathbf{x})$ is contaminated by Gaussian noise $\zeta \sim \mathcal{N}(0.0, 0.2)$.
100 The maximal number of FEs is set to $N_{FE} = 50n$, with $5n$ allocated to initialization.
- 101 • Reinforcement learning (RL): We examine two RL tasks chosen from OpenAI Gym [2]:
102 Lunar Lander with $n = 12$ and Swimmer with $n = 16$. We set $N_{FE} = 50n$, with $5n$ FEs
103 allocated to initialization.
- 104 • Hyperparameter optimization (HPO): We consider 5 HPO tasks (task ID:
105 $\{53, 10101, 167149, 167162, 167170\}$) picked up from the HPOBench [3] for tun-
106 ing support vector machine (SVM) with $n = 2$, multi-layer perceptron (MLP) with $n = 5$,
107 random forest with $n = 4$ and XGBoost with $n = 8$. The computational budget is set the
108 same as in the RL tasks.

109 3.2 Ablation Experiments of the Initialization Strategies for L-BFGS

110 As discussed in Remark 2 of Section 2.2 in the main manuscript, we suggest initializing L-BFGS
111 at the point of $\arg\max_{\mathbf{x} \in \tilde{\Omega}} \underline{\sigma}^2(\mathbf{x})$, where $\underline{\sigma}^2(\mathbf{x})$ denotes the lower bound of $\sigma^2(\mathbf{x})$ over $\tilde{\Omega}$, to ensure the
112 numerical stability of $\tilde{\mathbf{x}}$. To validate the effectiveness of this initialization strategy, we compare it
113 with regard to a variant (dubbed Random) that samples a randomly generated solution from $\tilde{\Omega}$ as the
114 starting point. From the statistical comparison results shown in Table 1, we can see that our proposed
115 initialization strategy outperforms Random. More specifically, it achieves statistically significant
116 better median regrets in more than half of the comparisons. Note that even Random can obtain better
117 regret than ours, many of them do not have statistical significance.

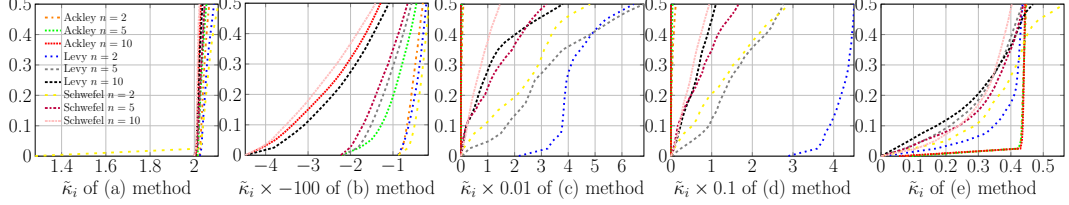


Figure 1: Trajectories of I_{cdf} obtained by applying UCB to solve synthetic functions. Different subplots are (a) our proposed method, (b) Naïve method, (c) Nguyen’s method, (d) Lorenz’s method, and (e) Makarova’s method, respectively.

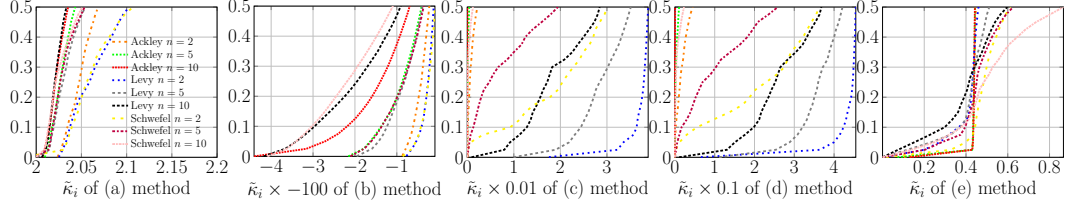


Figure 2: Trajectories of I_{cdf} obtained by applying EI to solve synthetic functions. Different subplots are (a) our proposed method, (b) Naïve method, (c) Nguyen’s method, (d) Lorenz’s method, and (e) Makarova’s method, respectively.

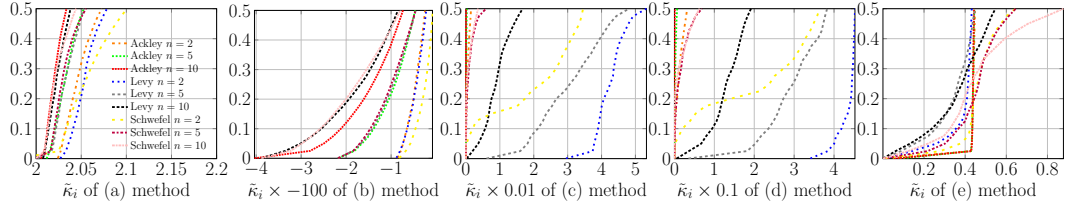


Figure 3: Trajectories of I_{cdf} obtained by applying PI to solve synthetic functions. Different subplots are (a) our proposed method, (b) Naïve method, (c) Nguyen’s method, (d) Lorenz’s method, and (e) Makarova’s method, respectively.

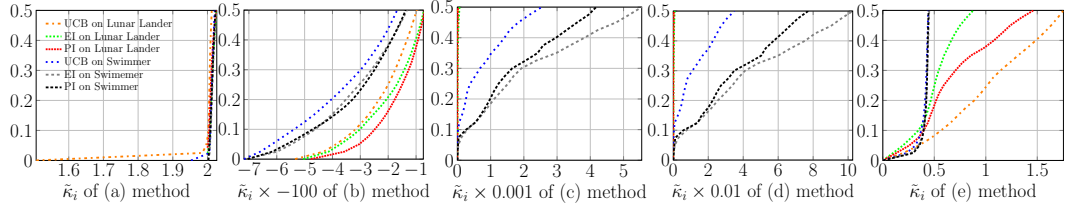


Figure 4: Trajectories of I_{cdf} obtained by applying UCB, EI, PI to solve RL problems. Different subplots are (a) our proposed method, (b) Naïve method, (c) Nguyen’s method, (d) Lorenz’s method, and (e) Makarova’s method, respectively.

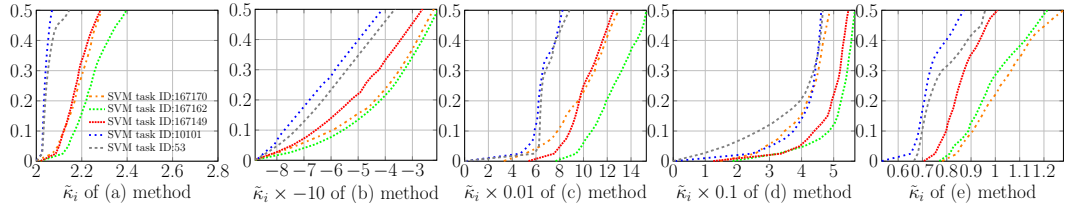


Figure 5: Trajectories of I_{cdf} obtained by applying UCB to tune SVM on different tasks. Different subplots are (a) our proposed method, (b) Naïve method, (c) Nguyen’s method, (d) Lorenz’s method, and (e) Makarova’s method, respectively.

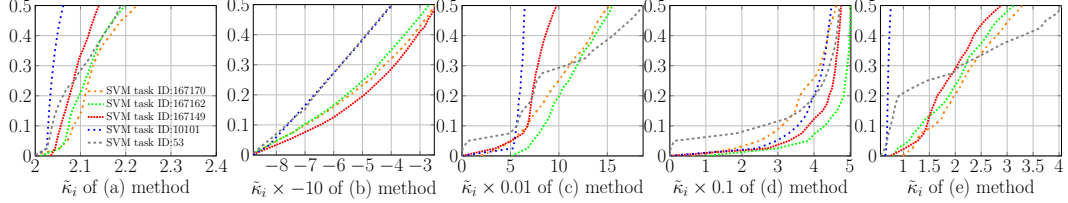


Figure 6: Trajectories of I_{cdf} obtained by applying EI to tune SVM on different tasks. Different subplots are (a) our proposed method, (b) Naïve method, (c) Nguyen’s method, (d) Lorenz’s method, and (e) Makarova’s method, respectively.

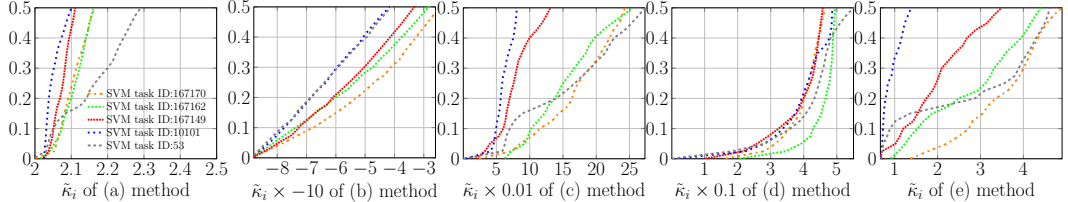


Figure 7: Trajectories of I_{cdf} obtained by applying PI to tune SVM on different tasks. Different subplots are (a) our proposed method, (b) Naïve method, (c) Nguyen’s method, (d) Lorenz’s method, and (e) Makarova’s method, respectively.

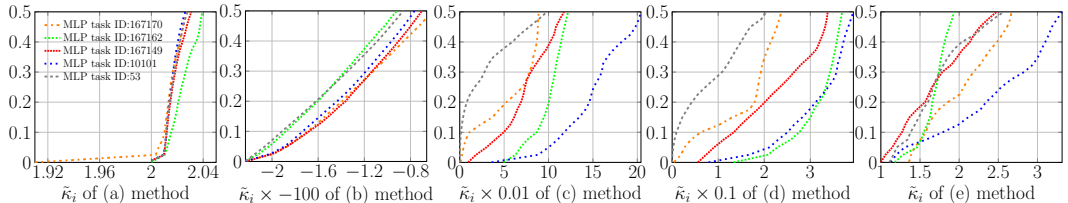


Figure 8: Trajectories of I_{cdf} obtained by applying UCB to tune MLP on different tasks. Different subplots are (a) our proposed method, (b) Naïve method, (c) Nguyen’s method, (d) Lorenz’s method, and (e) Makarova’s method, respectively.

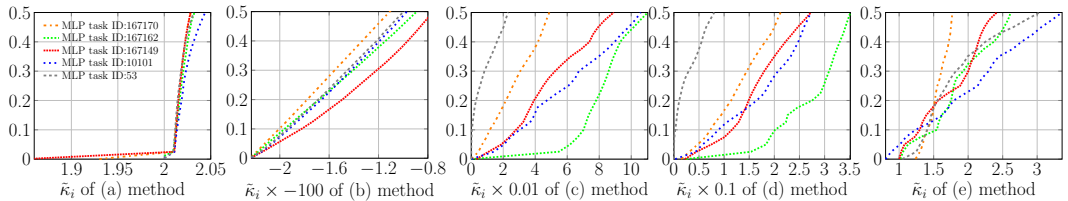


Figure 9: Trajectories of I_{cdf} obtained by applying EI to tune MLP on different tasks. Different subplots are (a) our proposed method, (b) Naïve method, (c) Nguyen’s method, (d) Lorenz’s method, and (e) Makarova’s method, respectively.

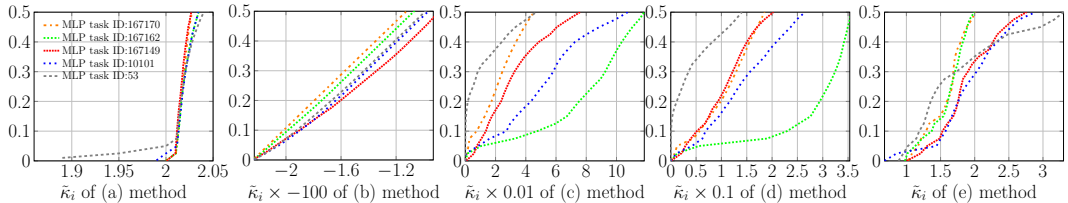


Figure 10: Trajectories of I_{cdf} obtained by applying PI to tune MLP on different tasks. Different subplots are (a) our proposed method, (b) Naïve method, (c) Nguyen’s method, (d) Lorenz’s method, and (e) Makarova’s method, respectively.

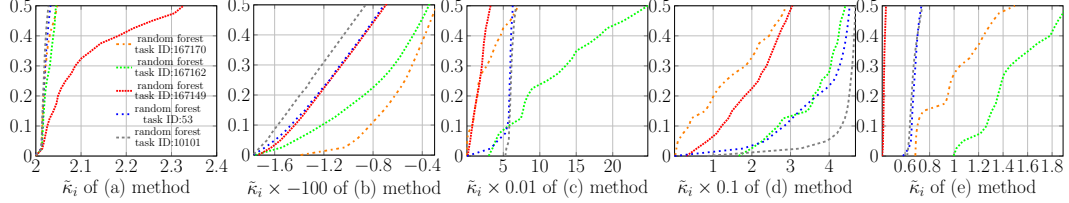


Figure 11: Trajectories of I_{cdf} obtained by applying UCB to tune random forest on different tasks. Different subplots are (a) our proposed method, (b) Naïve method, (c) Nguyen’s method, (d) Lorenz’s method, and (e) Makarova’s method, respectively.

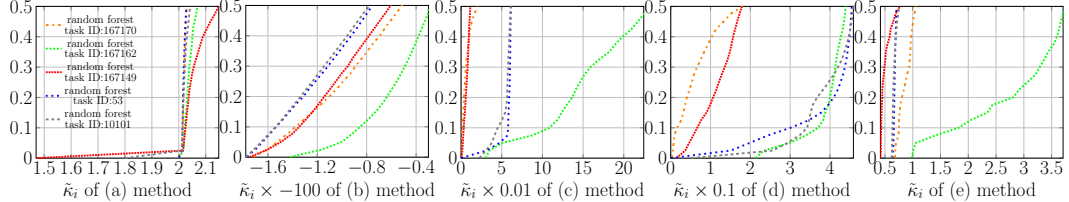


Figure 12: Trajectories of I_{cdf} obtained by applying EI to tune random forest on different tasks. Different subplots are (a) our proposed method, (b) Naïve method, (c) Nguyen’s method, (d) Lorenz’s method, and (e) Makarova’s method, respectively.

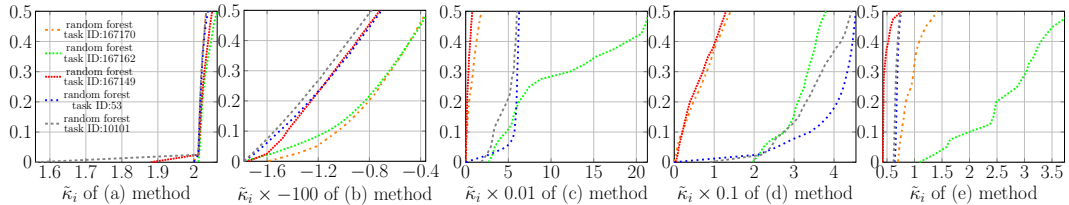


Figure 13: Trajectories of I_{cdf} obtained by applying PI to tune random forest on different tasks. Different subplots are (a) our proposed method, (b) Naïve method, (c) Nguyen’s method, (d) Lorenz’s method, and (e) Makarova’s method, respectively.

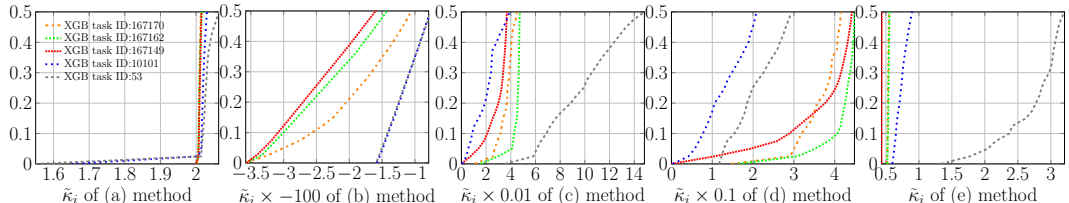


Figure 14: Trajectories of I_{cdf} obtained by applying UCB to tune XGBoost on different tasks. Different subplots are (a) our proposed method, (b) Naïve method, (c) Nguyen’s method, (d) Lorenz’s method, and (e) Makarova’s method, respectively.

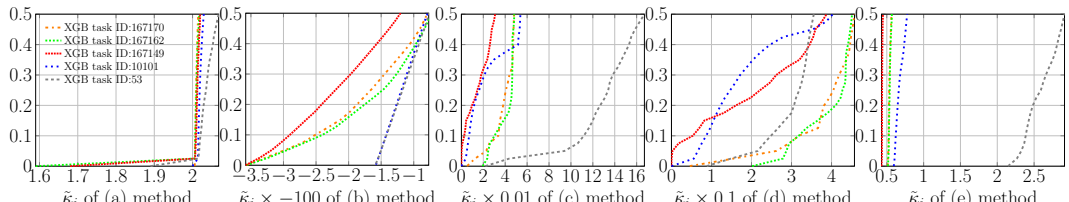


Figure 15: Trajectories of I_{cdf} obtained by applying EI to tune XGBoost on different tasks. Different subplots are (a) our proposed method, (b) Naïve method, (c) Nguyen’s method, (d) Lorenz’s method, and (e) Makarova’s method, respectively.

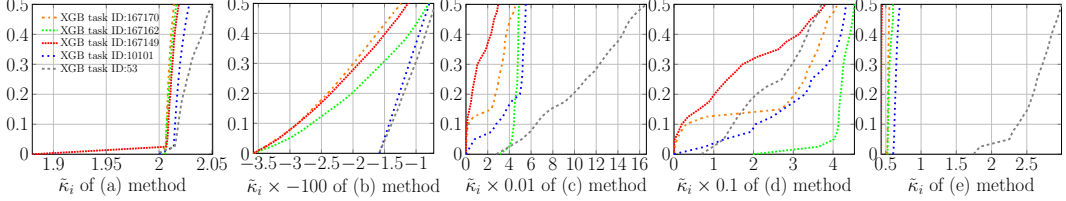


Figure 16: Trajectories of L_{cdf} obtained by applying PI to tune XGBoost on different tasks. Different subplots are (a) our proposed method, (b) Naïve method, (c) Nguyen’s method, (d) Lorenz’s method, and (e) Makarova’s method, respectively.

Table 1: The statistical comparison results of different initialization strategies in L-BFGS.

	Ackley ($n = 2$)	Ackley ($n = 5$)	Ackley ($n = 10$)	Levy ($n = 2$)
Our	0.6151(1.59E-1)*	0.7458(2.19E-1)*	0.6599(1.82E-1)†	0.322(1.60E-1)*
Random	0.7348(1.30E-1)	0.846(1.89E-1)	0.6406(1.92E-1)	0.337(1.82E-1)
	Levy ($n = 5$)	Levy ($n = 10$)	Schwefel ($n = 2$)	Schwefel ($n = 5$)
Our	0.7557(1.51E-1)*	0.7655(1.20 E - 1)†	0.8311(9.36 E - 2)†	0.8179(9.54E-2)†
Random	0.6966(1.61E-1)	0.679(1.01E-1)	0.7683(1.83E-1)	0.6804(2.92E-1)
	Schwefel ($n = 10$)	Lunar lander	Swimmer	SVM (Task #5)
Our	0.8515(7.81E-2)†	1.1246(2.68E-2)†	1.1071(2.02E-2)†	0.6713(2.25E-1)*
Random	0.478(2.35E-1)	1.1166(3.10E-2)	1.1009(1.65E-2)	0.5905(2.34E-1)
	SVM (Task #2)	SVM (Task #3)	SVM (Task #4)	SVM (Task #5)
Our	0.6574(1.84E-1)*	0.4855(1.43E-1)†	0.7607(1.98E-1)*	0.6349(2.01E-1)†
Random	0.5228(2.14E-1)	0.3722(1.95E-1)	0.5971(2.38E-1)	0.4865(2.01E-1)
	MLP (Task #1)	MLP (Task #2)	MLP (Task #3)	MLP (Task #4)
Our	0.9063(1.56E-1)†	0.8762(1.20E-1)†	0.9029(1.54E-1)†	0.8767(6.47E-2)*
Random	0.8359(1.77E-1)	0.7995(1.56E-1)	0.8279(3.06E-1)	0.8108(1.13E-1)
	MLP (Task #5)	Random forest (Task #1)	Random forest (Task #2)	Random forest (Task #3)
Our	0.8879(1.50E-1)†	0.3479(1.39E-1)*	0.3493(1.76E-1)*	0.3377(1.79E-1)†
Random	0.817(2.47E-1)	0.2927(1.99E-1)	0.3493(1.65E-1)	0.3414(1.20E-1)
	Random forest (Task #4)	Random forest (Task #5)	XGBoost (Task #1)	XGBoost (Task #2)
Our	0.3242(1.26E-1)†	0.3841(9.13E-2)*	0.8762(2.19E-1)*	0.8601(2.01E-1)†
Random	0.2903(9.90E-2)	0.3841(1.56E-1)	0.8417(2.22E-1)	0.783(3.10E-1)
	XGBoost (Task #3)	XGBoost (Task #4)	XGBoost (Task #5)	
Our	0.6982(2.36E-1)*	0.7185(2.55 E - 1)*	0.8375(1.58E-1)*	
Random	0.5493(2.27E-1)	0.583(2.69E-1)	0.6956(1.86E-1)	

† denotes the performance of our proposed initialization strategy is significantly better than the random initialization strategy according to the Wilcoxon’s rank sum test at a 0.05 significance level. Whereas * denotes the better result does not have any statistical significance. The Task #1 to the Task #5 corresponds to the task ID: {53, 10101, 167149, 167162, 167170} of HPOBench [3], respectively.

118 References

- 119 [1] Stephen Boyd and Lieven Vandenberghe. *Convex optimization*. Cambridge university press,
120 2004.
- 121 [2] Greg Brockman, Vicki Cheung, Ludwig Pettersson, Jonas Schneider, John Schulman, Jie Tang,
122 and Wojciech Zaremba. OpenAI Gym. Retrieved January 20, 2023, from <https://github.com/openai/gym>.
- 123 [3] Katharina Eggensperger, Philipp Müller, Neeratyoy Mallik, Matthias Feurer, Rene Sass, Aaron
125 Klein, Noor Awad, Marius Lindauer, and Frank Hutter. HPOBench: A collection of reproducible

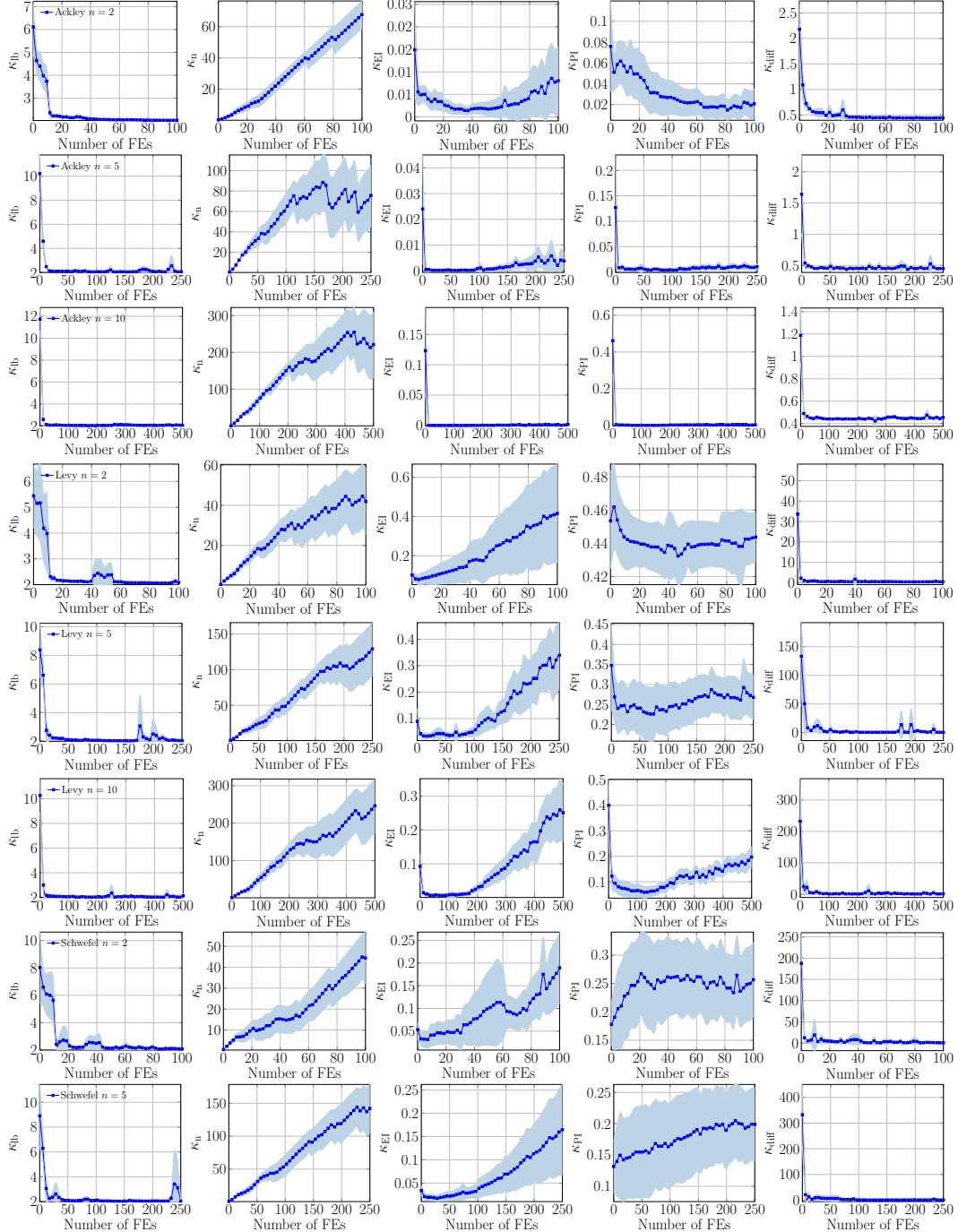


Figure 17: Trajectories of different termination indicators versus the number of FEs during the BO process of applying UCB on Ackley ($n \in \{2, 5, 10\}$), Levy ($n \in \{2, 5, 10\}$) and Schwefel ($n \in \{2, 5\}$).

126 multi-fidelity benchmark problems for HPO. In *NIPS’21: Proc. of the Thirty-fifth Conference on*
 127 *Neural Information Processing Systems Datasets and Benchmarks Track (Round 2)*, 2021.

128 [4] P. Langley. Crafting papers on machine learning. In Pat Langley, editor, *ICML’00: Proc. of*
 129 *the 17th International Conference on Machine Learning*, pages 1207–1216, Stanford, CA, 2000.
 130 Morgan Kaufmann.

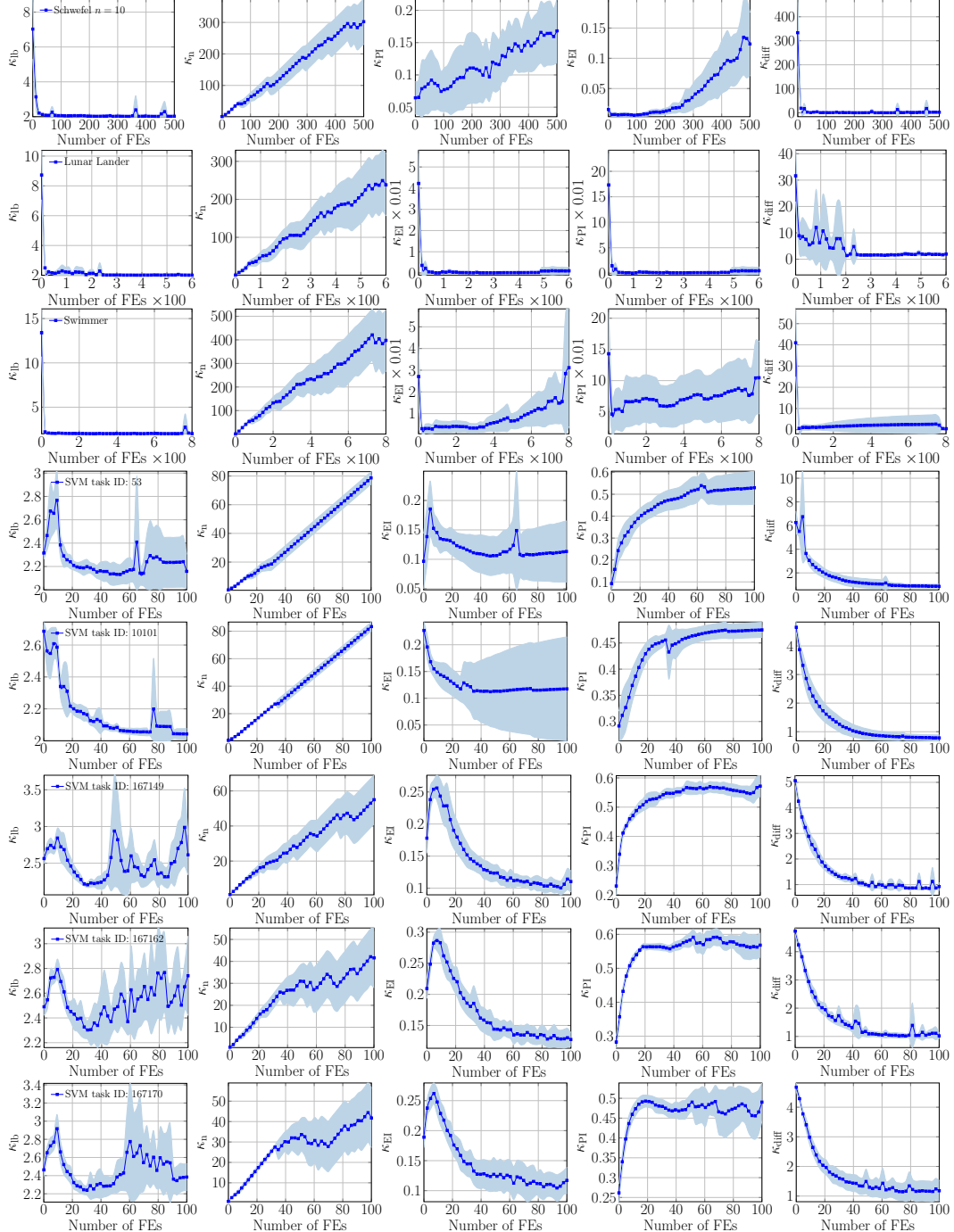


Figure 18: Trajectories of different termination indicators versus the number of FEs during the BO process of applying UCB on Schwefel ($n = 10$), Lunar Lander, Swimmer and SVM (task ID: {53, 10101, 167149, 167162, 167170}).

- 131 [5] Niranjan Srinivas, Andreas Krause, Sham M. Kakade, and Matthias W. Seeger. Information-
 132 theoretic regret bounds for gaussian process optimization in the bandit setting. *IEEE Trans. Inf.
 133 Theory*, 58(5):3250–3265, 2012.
- 134 [6] S. Surjanovic and D. Bingham. Virtual library of simulation experiments: Test functions and
 135 datasets. Retrieved January 20, 2023, from <http://www.sfu.ca/~ssurjano>.

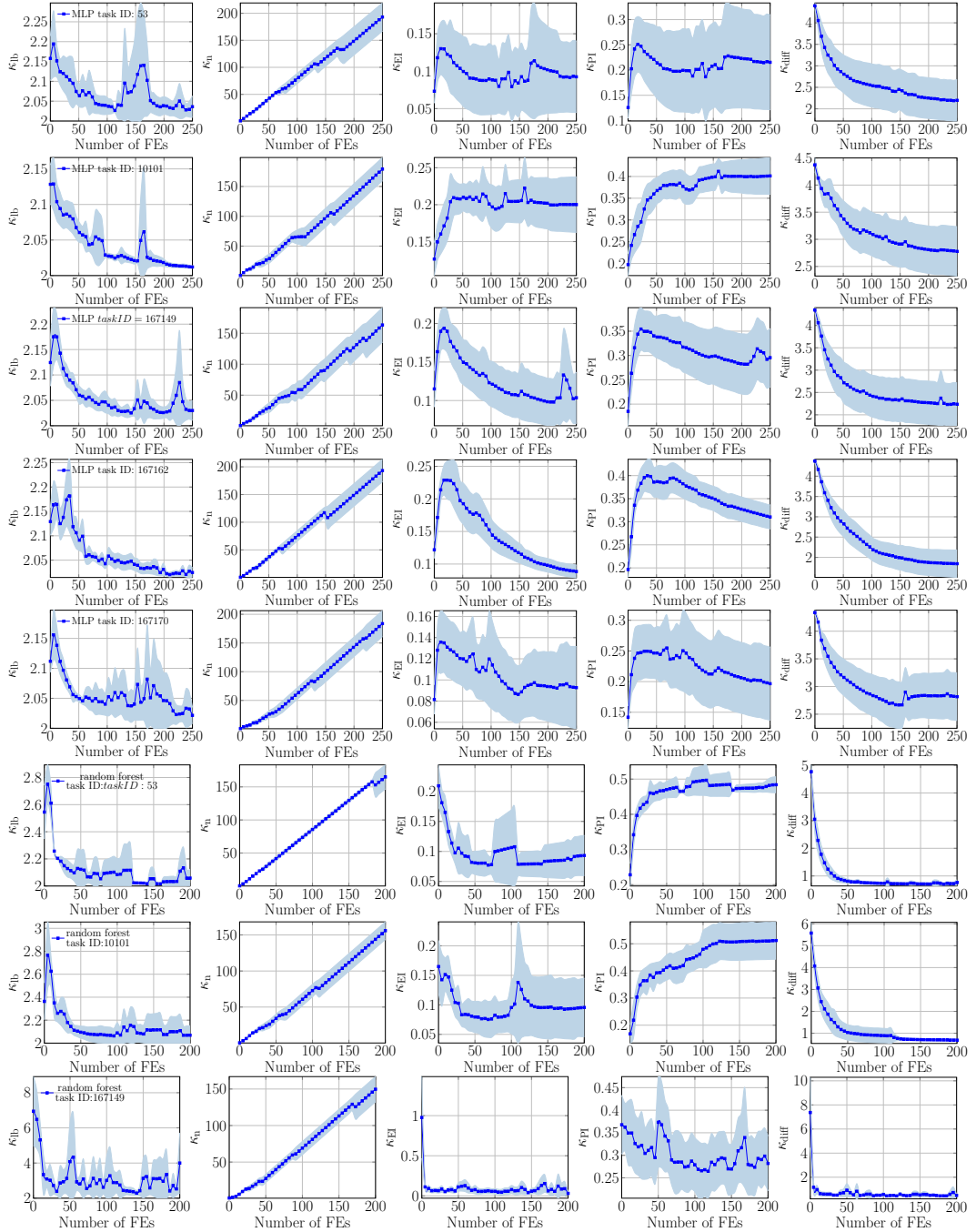


Figure 19: Trajectories of different termination indicators versus the number of FEs during the BO process of applying UCB on MLP (task ID: {53, 10101, 167149, 167162, 167170}) and random forest (task ID: {53, 10101, 167149}).

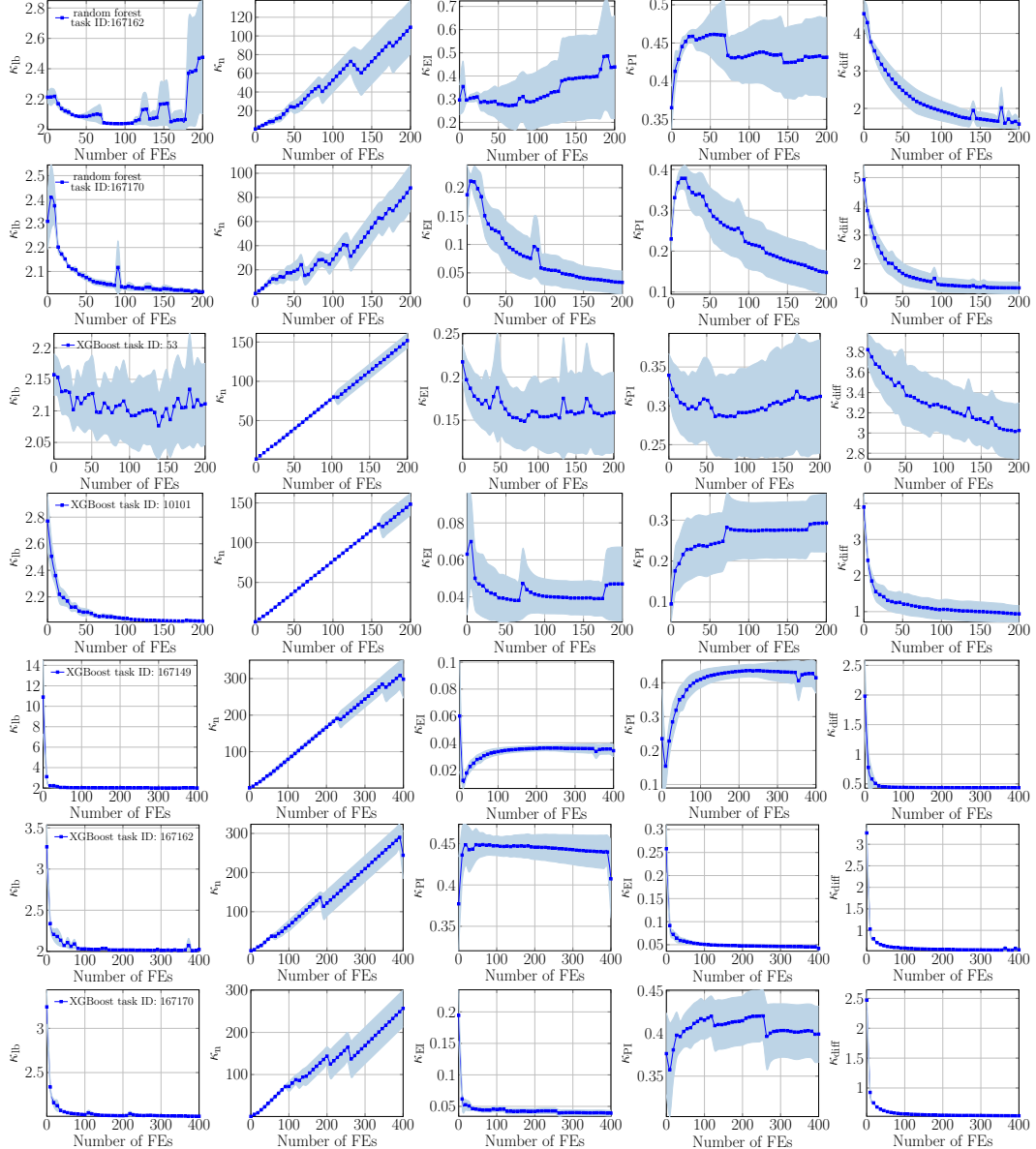


Figure 20: Trajectories of different termination indicators versus the number of FEs during the BO process of applying UCB on random forest (task ID: {167162, 167170}) and XGBoost (task ID: {53, 10101, 167149, 167162, 167170}).

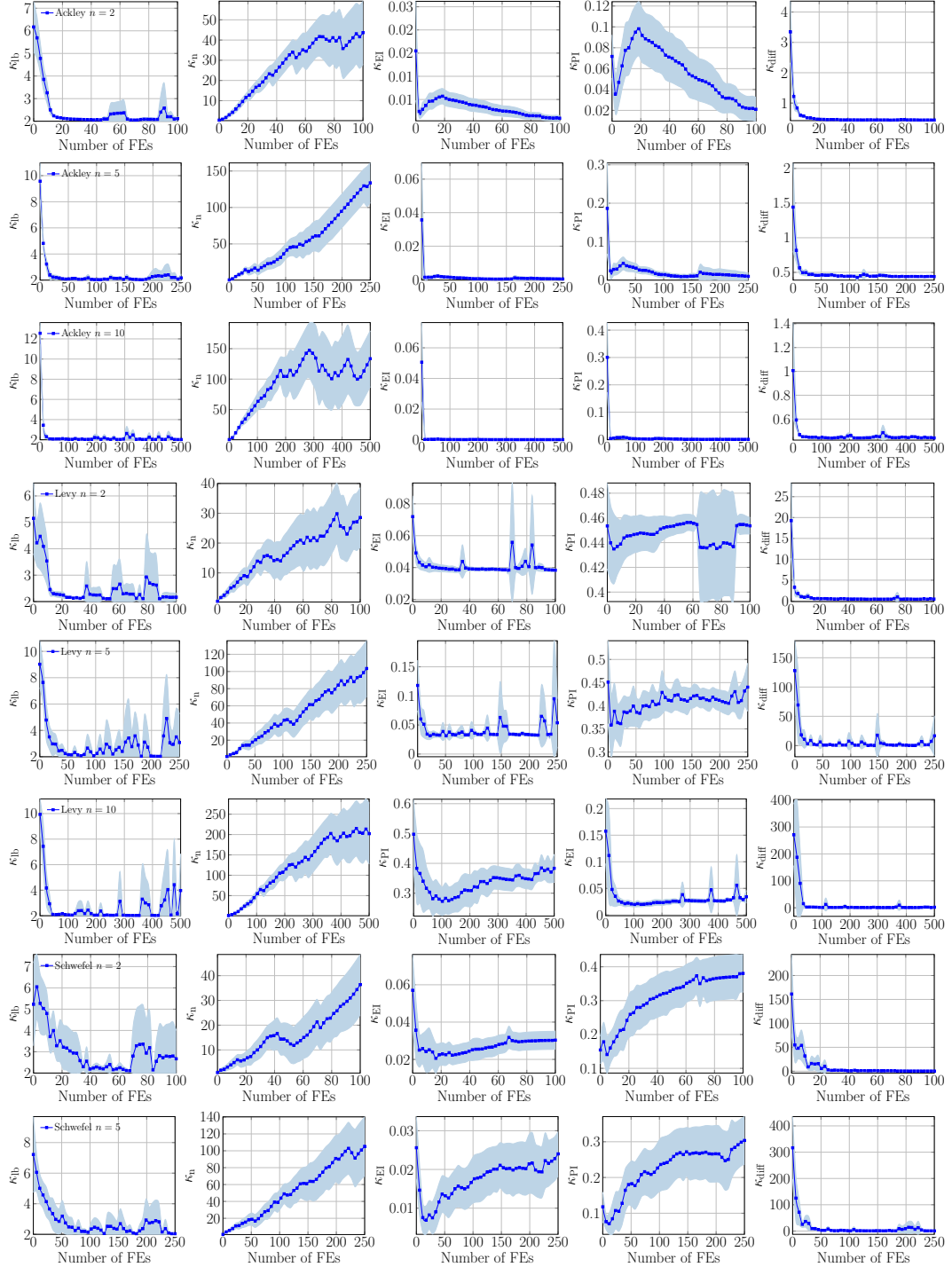


Figure 21: Trajectories of different termination indicators versus the number of FEs during the BO process of applying EI on Ackley ($n \in \{2, 5, 10\}$), Levy ($n \in \{2, 5, 10\}$) and Schwefel ($n \in \{2, 5\}$).

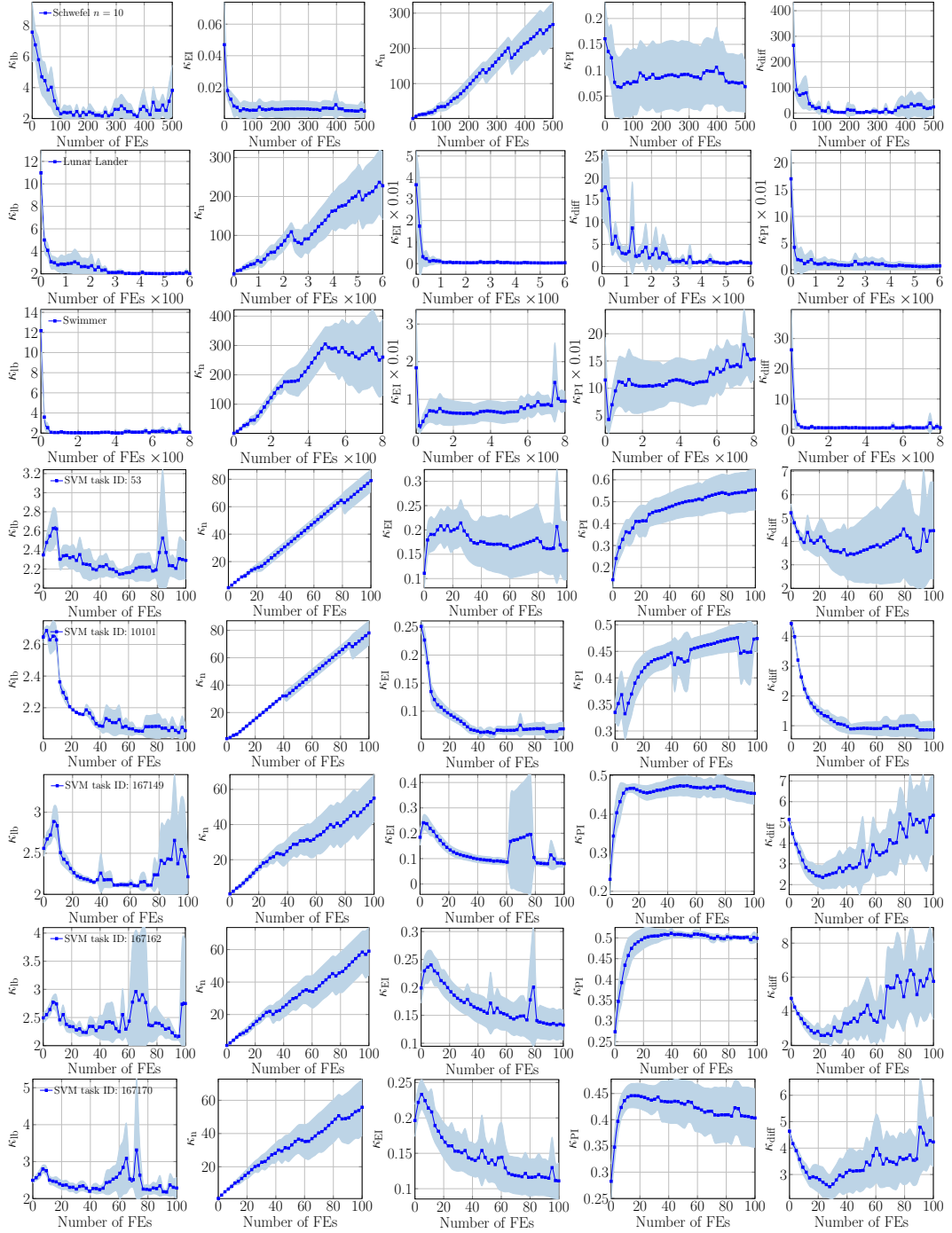


Figure 22: Trajectories of different termination indicators versus the number of FEs during the BO process of applying EI on Schwefel ($n = 10$), Lunar Lander, Swimmer and SVM (task ID: {53, 10101, 167149, 167162, 167170}).

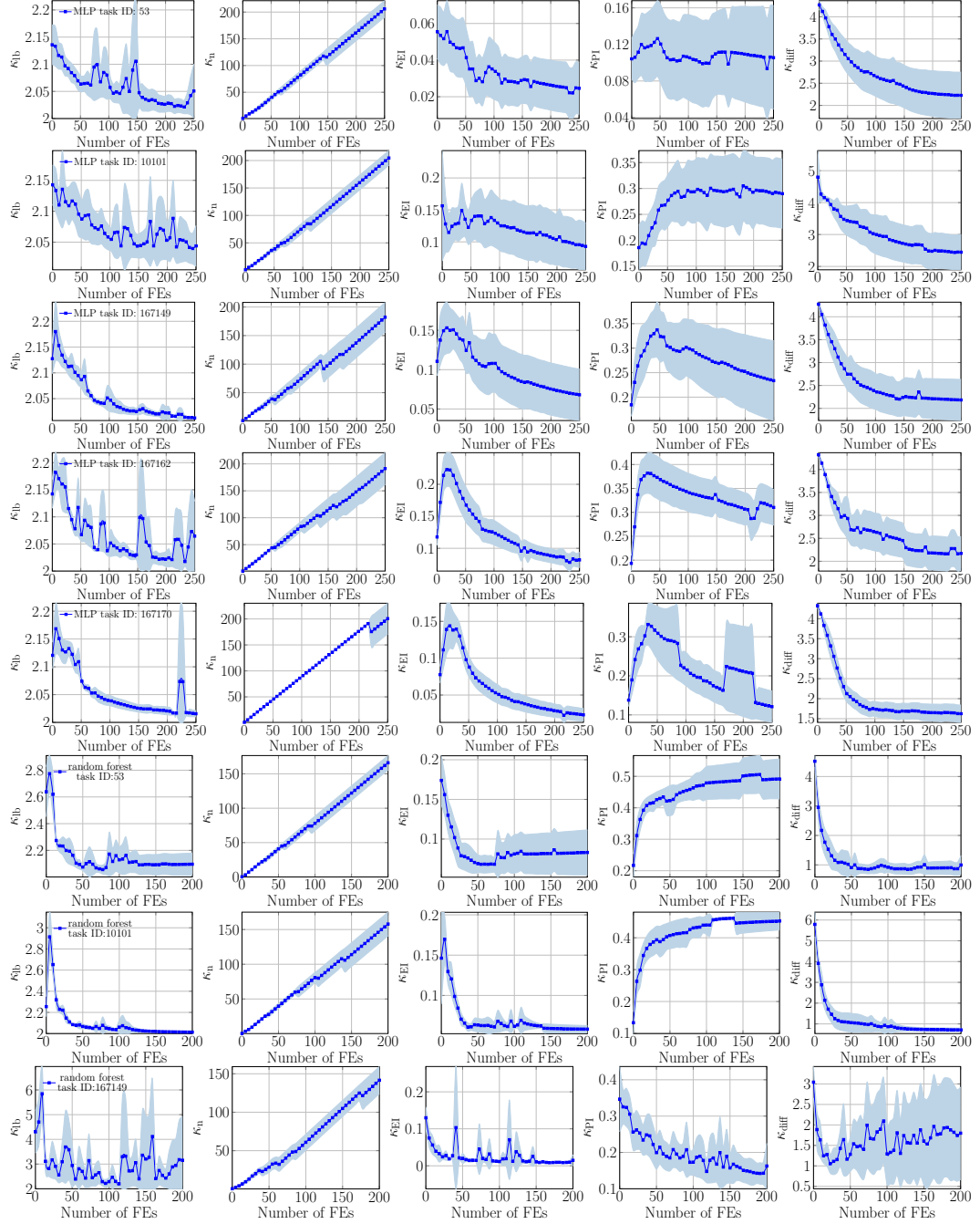


Figure 23: Trajectories of different termination indicators versus the number of FEs during the BO process of applying EI on MLP (task ID: {53, 10101, 167149, 167162, 167170}) and random forest (task ID: {53, 10101, 167149}).

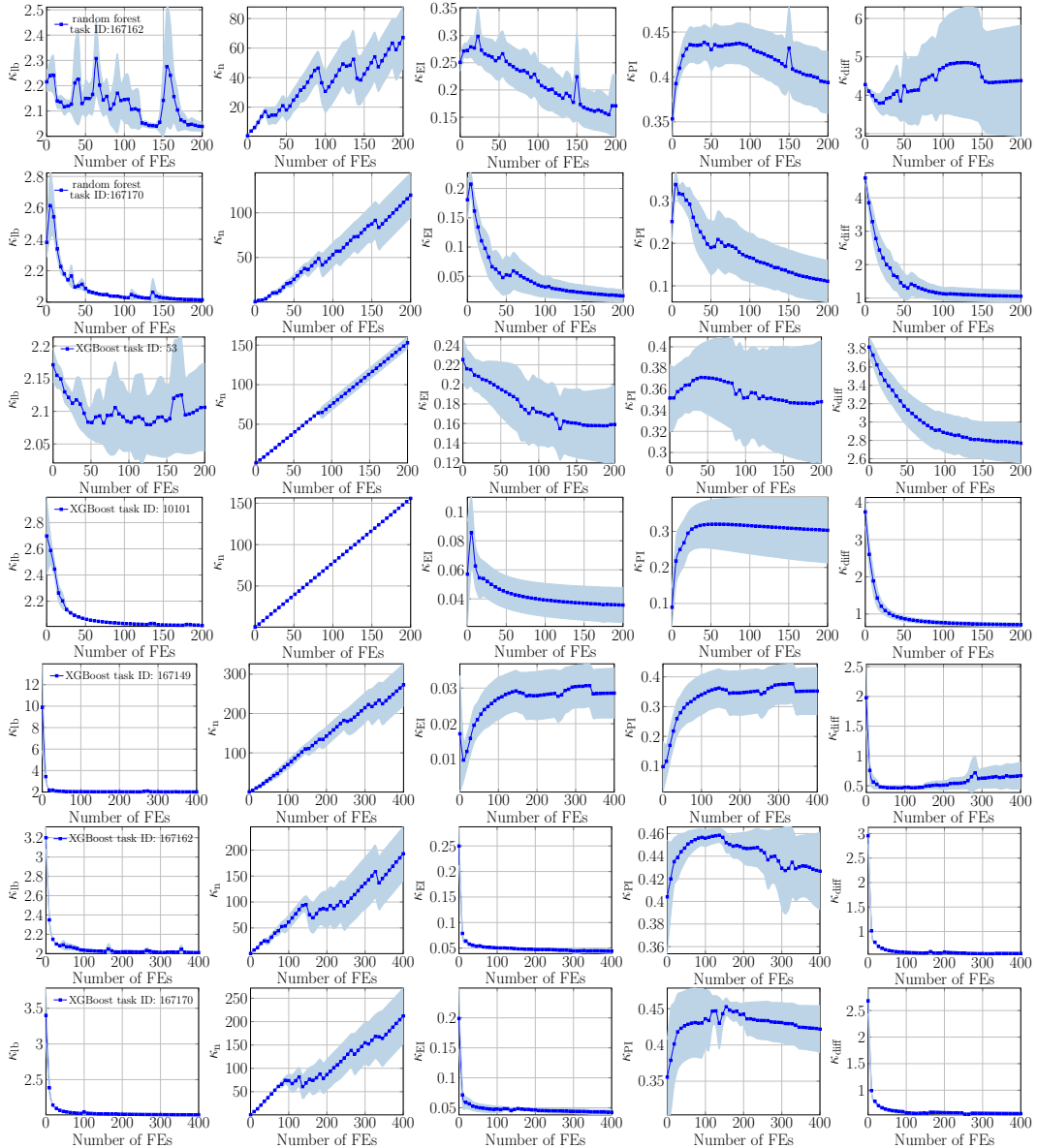


Figure 24: Trajectories of different termination indicators versus the number of FEs during the BO process of applying EI on random forest (task ID: {167162, 167170}) and XGBoost (task ID: {53, 10101, 167149, 167162, 167170}).

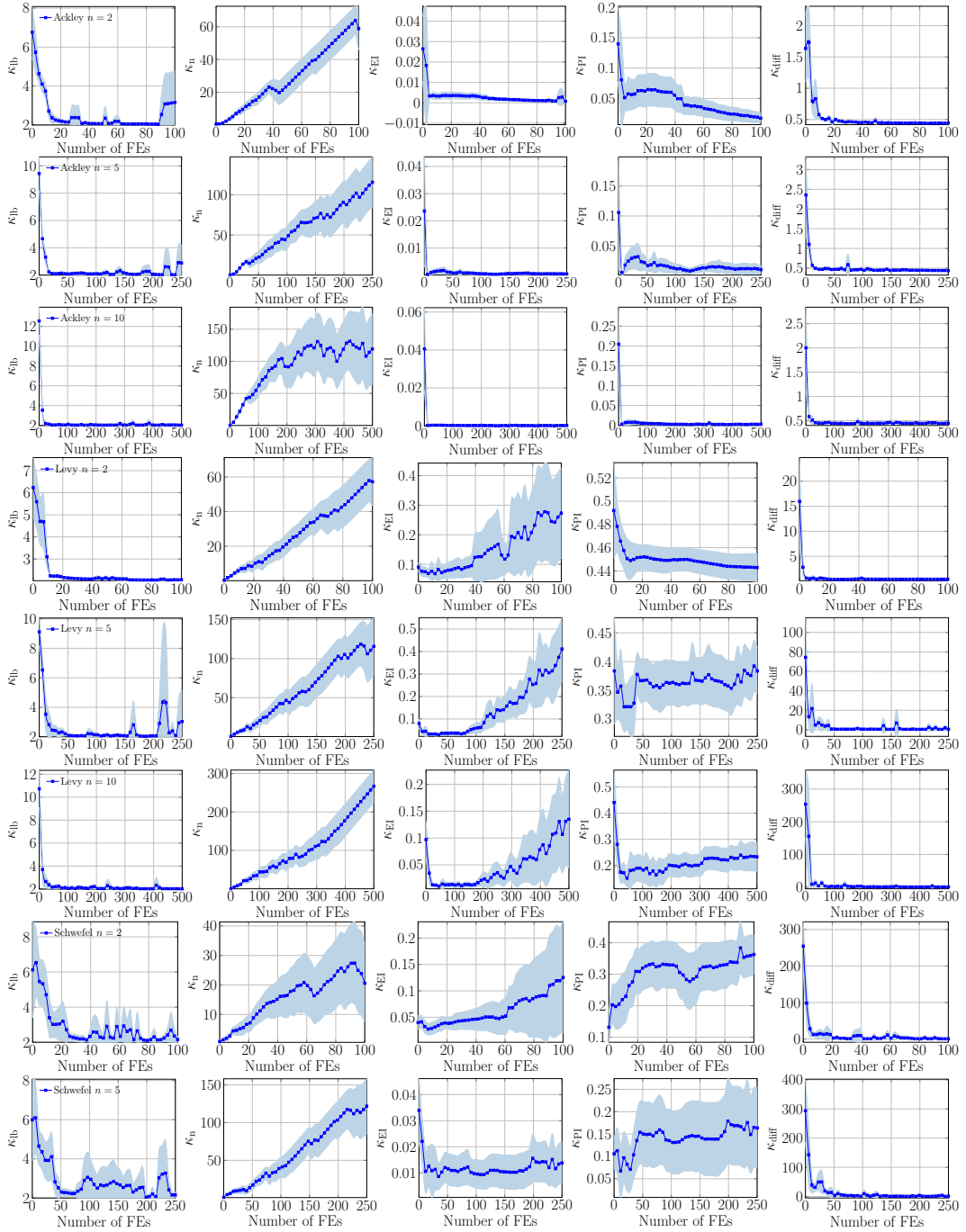


Figure 25: Trajectories of different termination indicators versus the number of FEs during the BO process of applying PI on Ackley ($n \in \{2, 5, 10\}$), Levy ($n \in \{2, 5, 10\}$) and Schwefel ($n \in \{2, 5\}$).

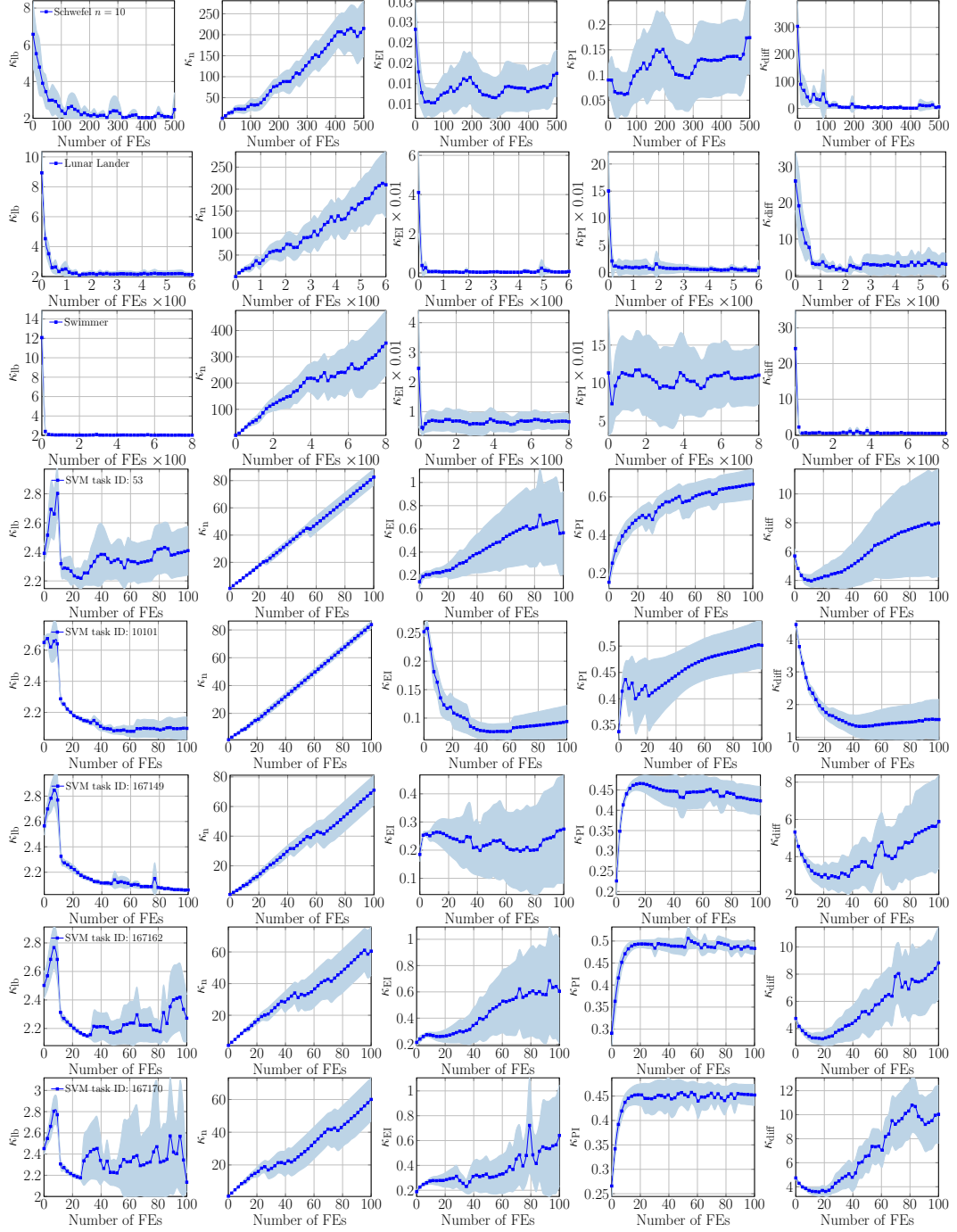


Figure 26: Trajectories of different termination indicators versus the number of FEs during the BO process of applying PI on Schwefel ($n = 10$), Lunar Lander, Swimmer and SVM (task ID: {53, 10101, 167149, 167162, 167170}).

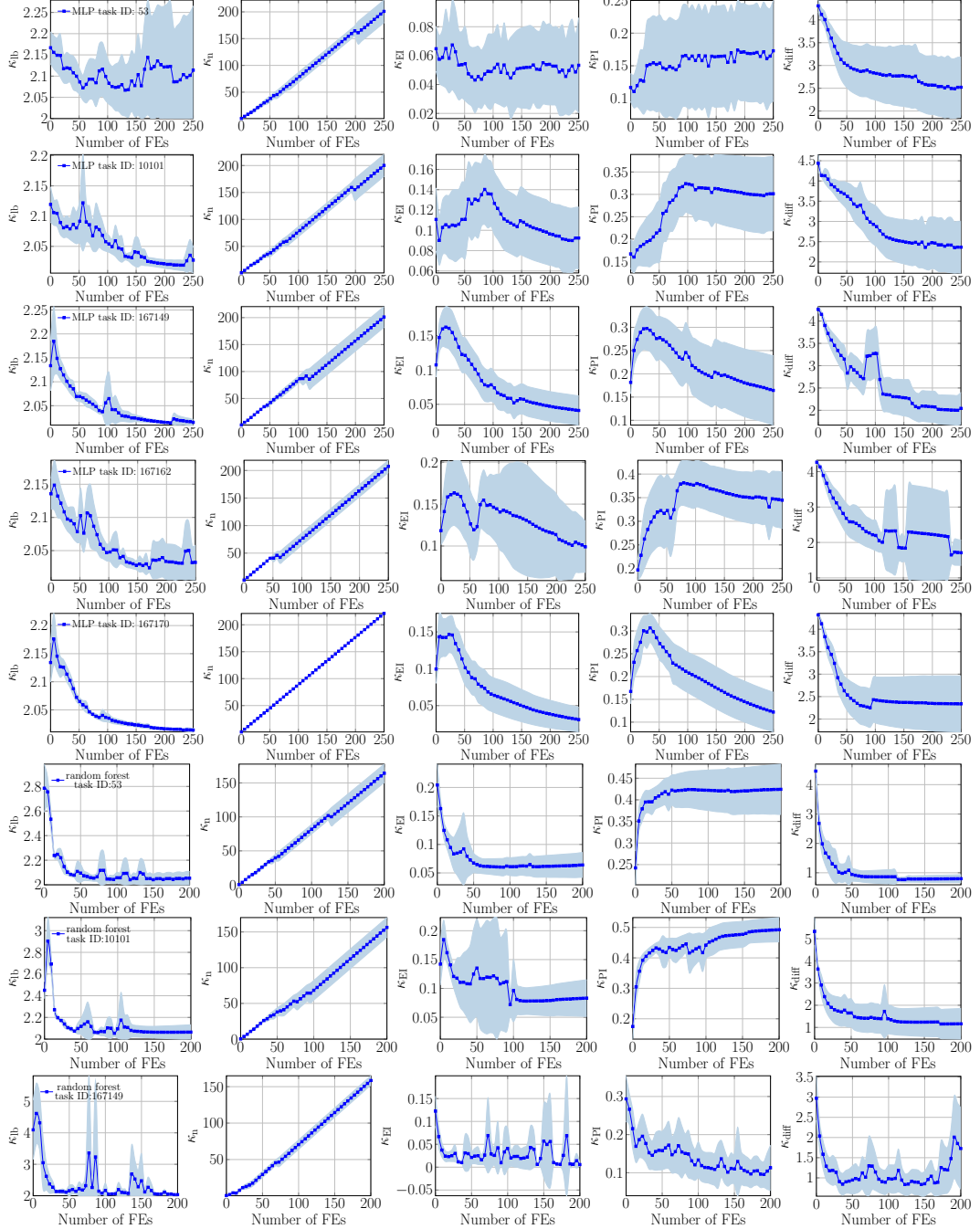


Figure 27: Trajectories of different termination indicators versus the number of FEs during the BO process of applying PI on MLP (task ID: {53, 10101, 167149, 167162, 167170}) and random forest (task ID: {53, 10101, 167149}).

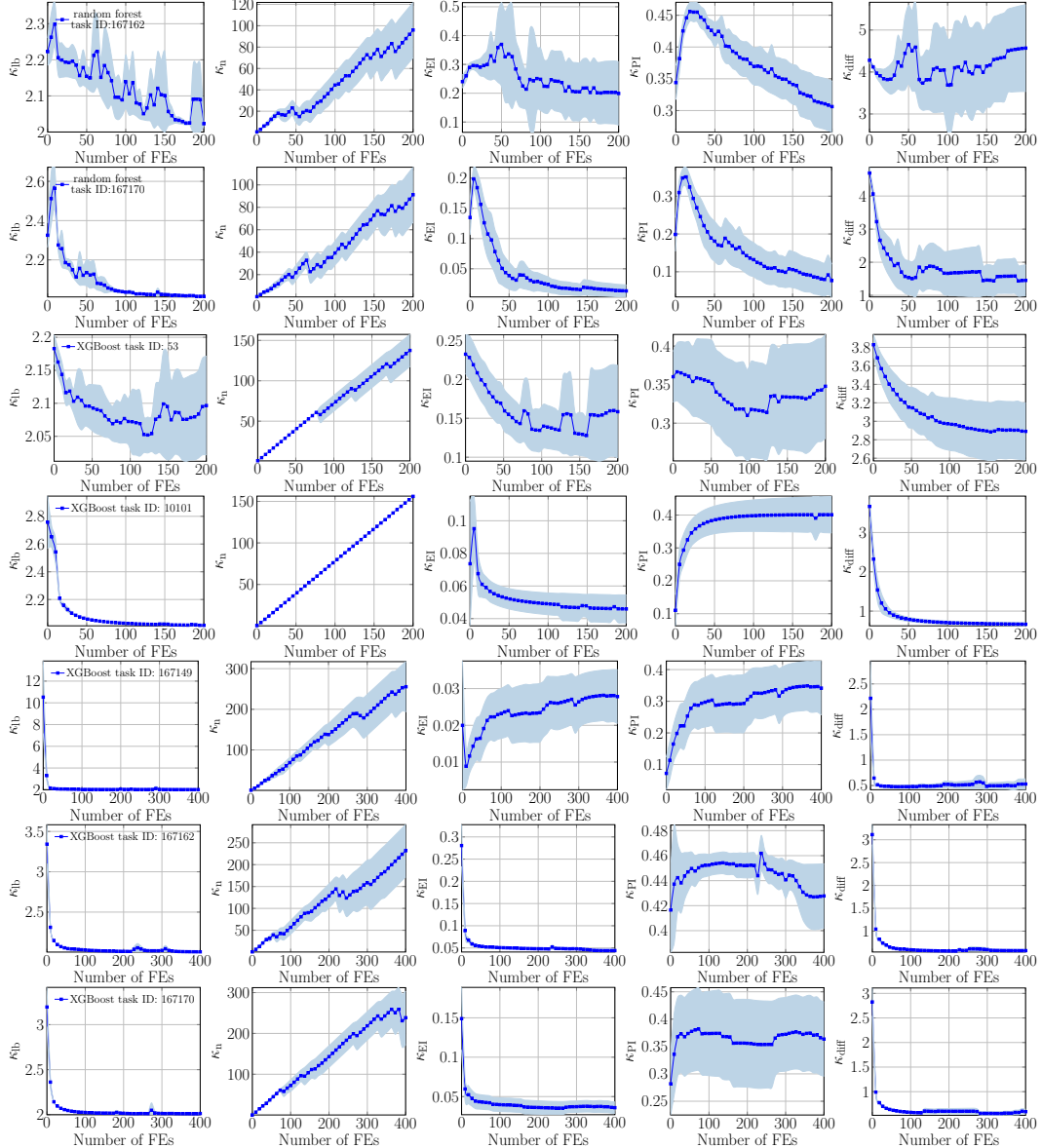


Figure 28: Trajectories of different termination indicators versus the number of FEs during the BO process of applying PI on random forest (task ID: {167162, 167170}) and XGBoost (task ID: {53, 10101, 167149, 167162, 167170}).

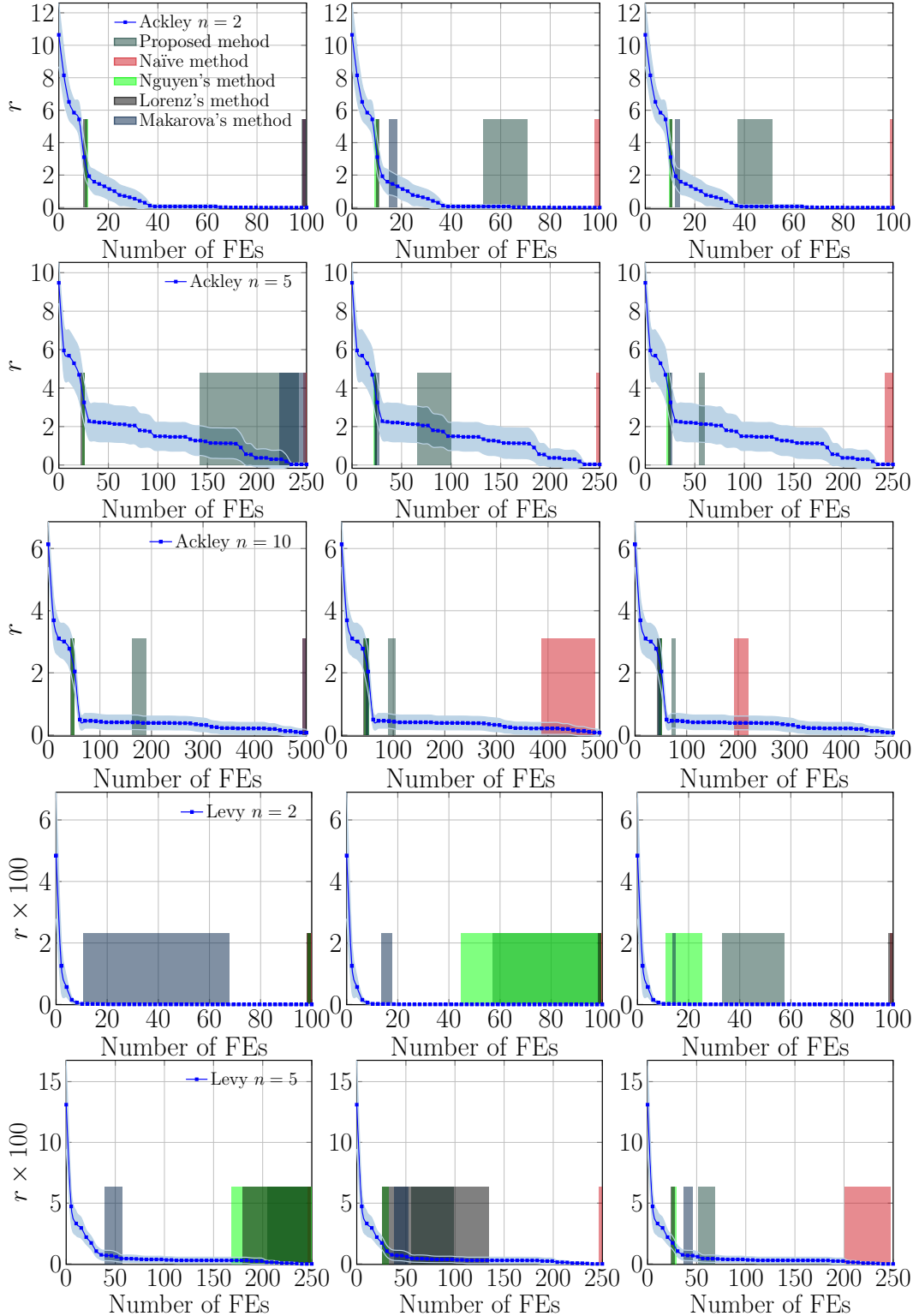


Figure 29: Trajectories of the regret of BO versus the number of FEs during the BO process of applying UCB on Ackley ($n \in \{2, 5, 10\}$) and Levy ($n \in \{2, 5\}$). The results of the first column, second column, and third column are obtained by using different settings of the termination threshold suggested in Section 3.2 of the main paper respectively.

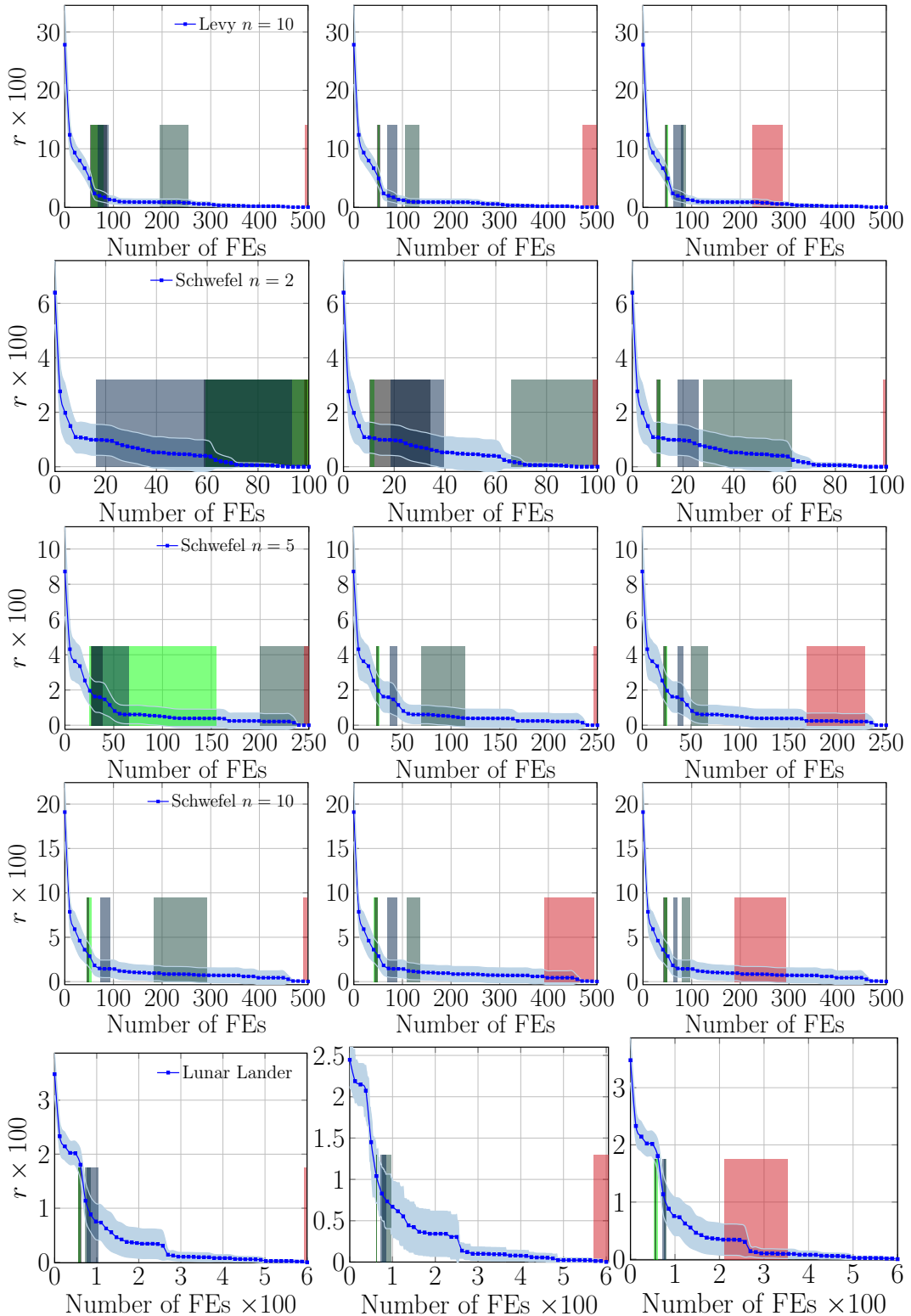


Figure 30: Trajectories of the regret of BO versus the number of FEs during the BO process of applying UCB on Levy ($n = 10$), Schwefel ($n \in \{2, 5, 10\}$) and Lunar Lander. The results of the first column, second column, and third column are obtained by using different settings of the termination threshold suggested in Section 3.2 of the main paper respectively.

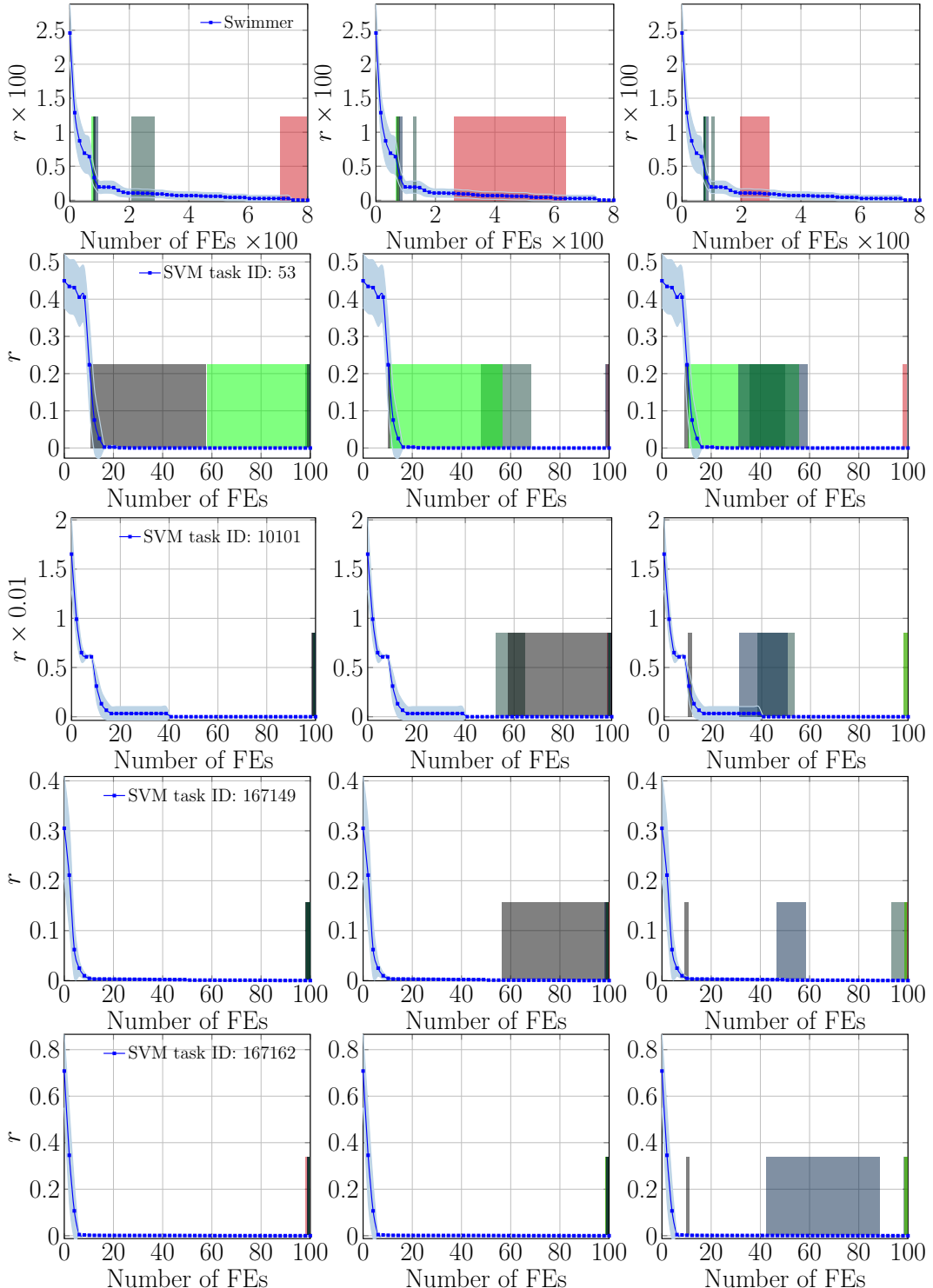


Figure 31: Trajectories of the regret of BO versus the number of FEs during the BO process of applying UCB on Swimmer and SVM (task ID: {53, 10101, 167149, 167162}). The results of the first column, second column, and third column are obtained by using different settings of the termination threshold suggested in Section 3.2 of the main paper respectively.

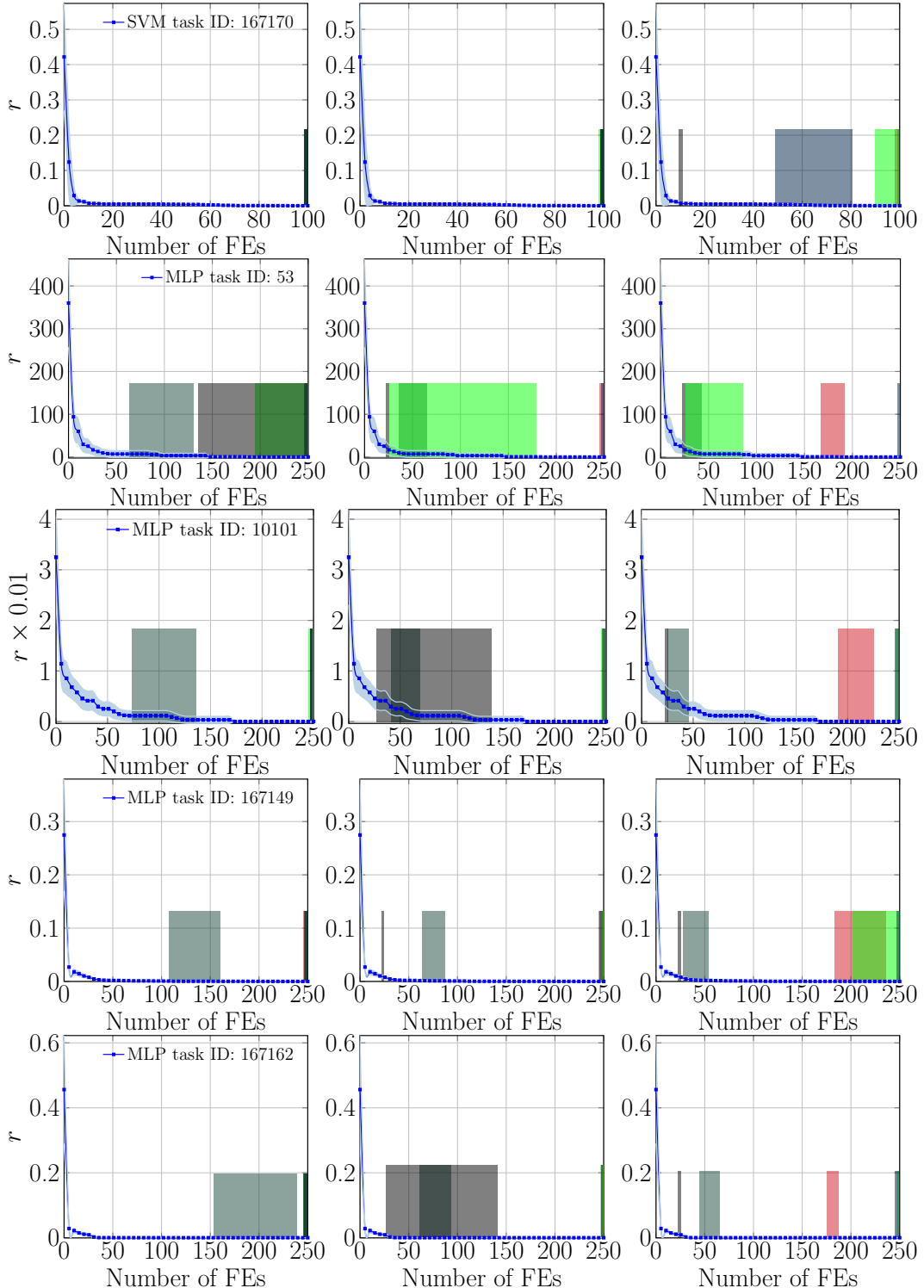


Figure 32: Trajectories of the regret of BO versus the number of FEs during the BO process of applying UCB on SVM (task ID: 167170) and MLP (task ID: {53, 10101, 167149, 167162}). The results of the first column, second column, and third column are obtained by using different settings of the termination threshold suggested in Section 3.2 of the main paper respectively.

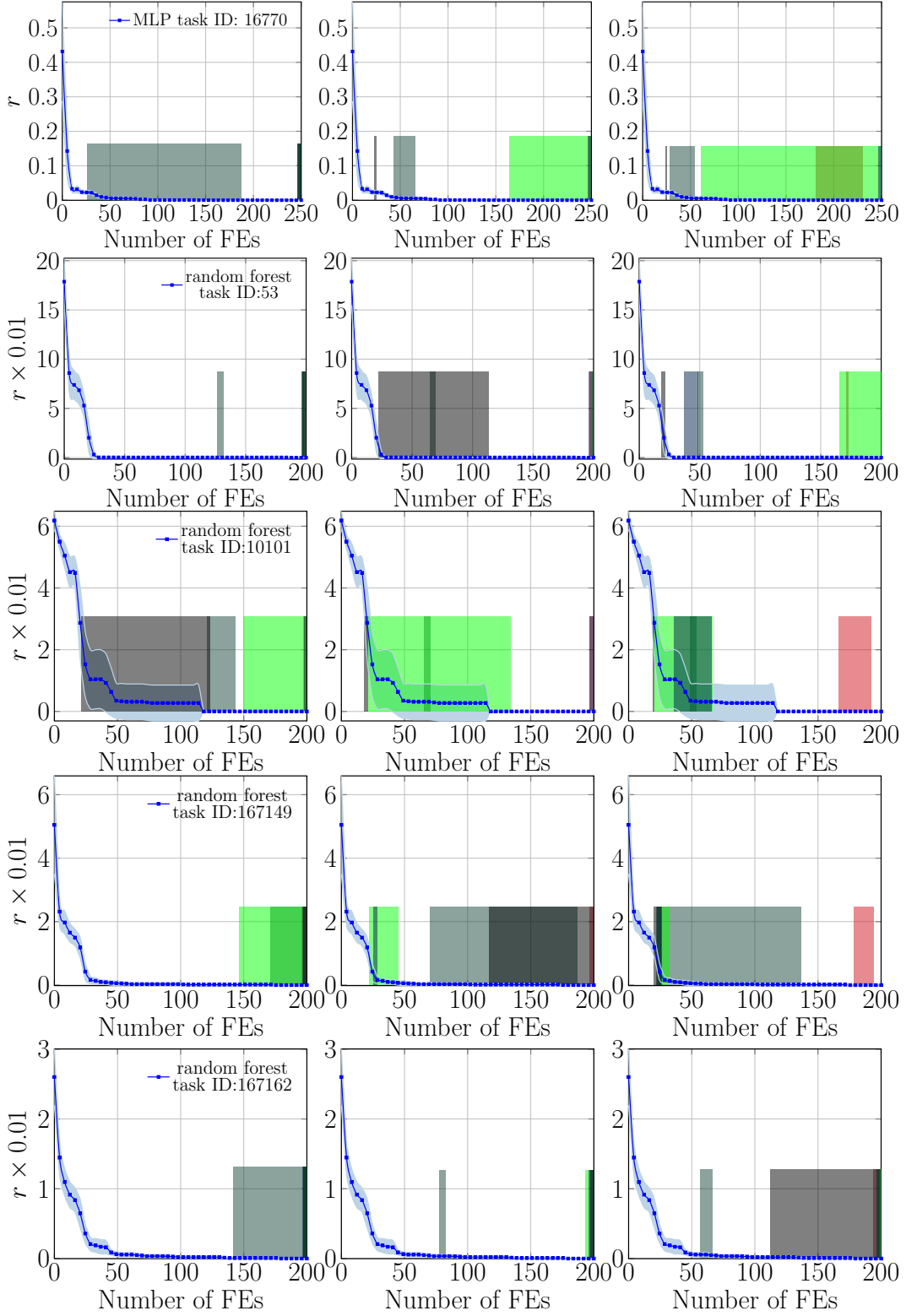


Figure 33: Trajectories of the regret of BO versus the number of FEs during the BO process of applying UCB on MLP (task ID: 167170) and random forest (task ID: {53, 10101, 167149, 167162}). The results of the first column, second column, and third column are obtained by using different settings of the termination threshold suggested in Section 3.2 of the main paper respectively.

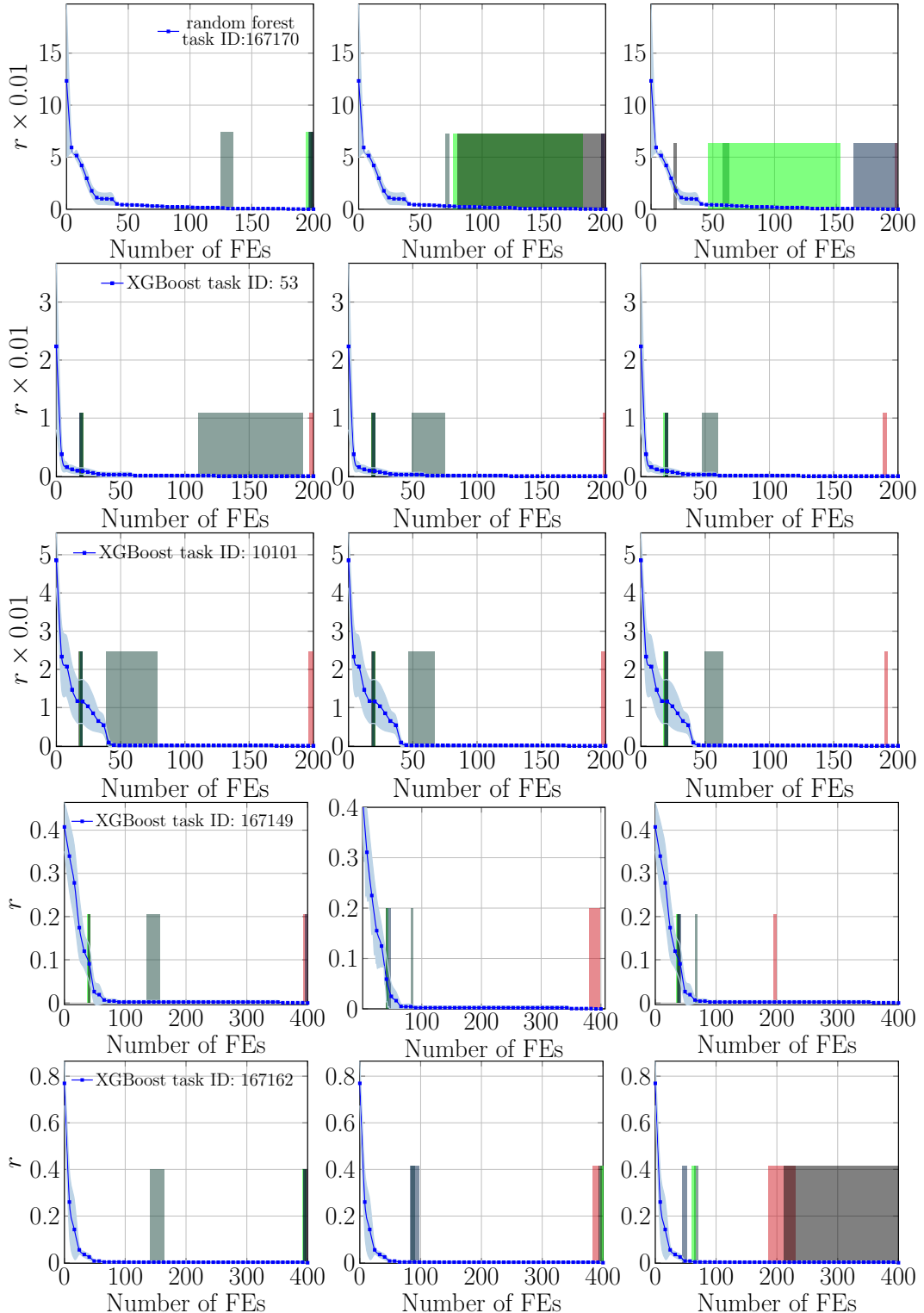


Figure 34: Trajectories of the regret of BO versus the number of FEs during the BO process of applying UCB on random forest (task ID: 167170) and XGBoost (task IDs: {53, 10101, 167149, 167162}). The results of the first column, second column, and third column are obtained by using different settings of the termination threshold suggested in Section 3.2 of the main paper respectively.

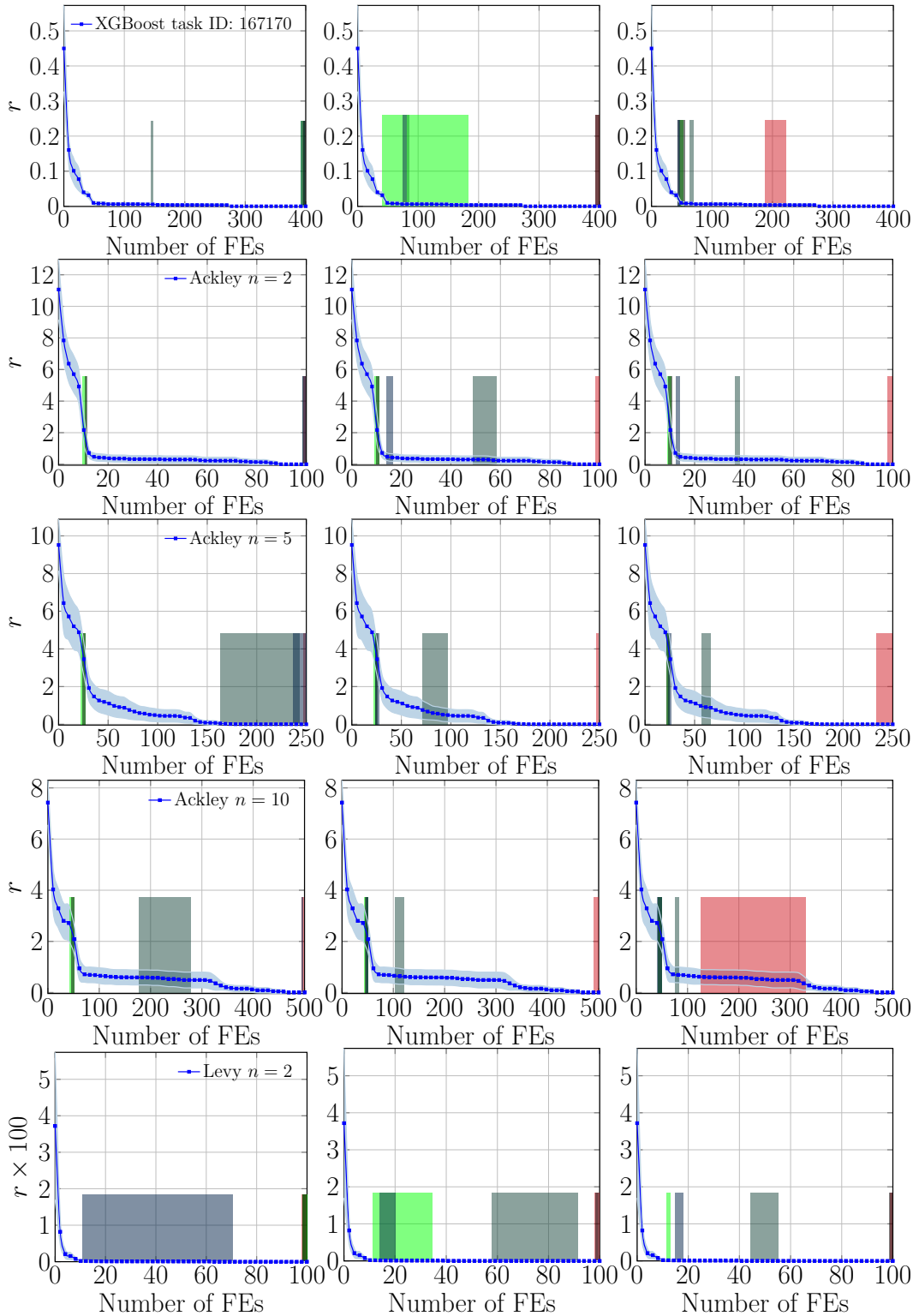


Figure 35: Trajectories of the regret of BO versus the number of FEs during the BO process of applying UCB on XGBoost (task ID: 167170), and applying EI on Ackley ($n \in \{2, 5, 10\}$) and Levy ($n = 2$). The results of the first column, second column, and third column are obtained by using different settings of the termination threshold suggested in Section 3.2 of the main paper respectively.

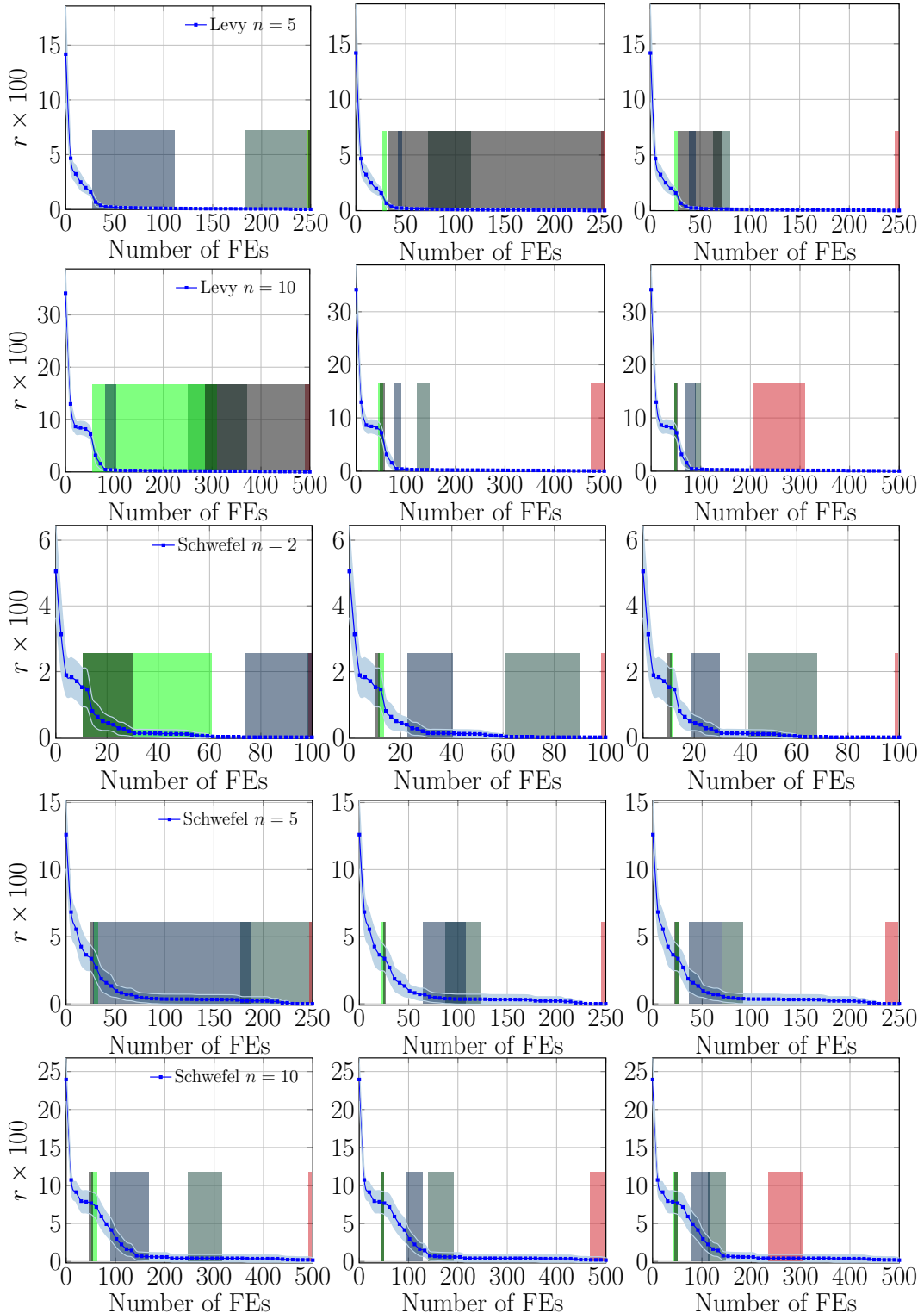


Figure 36: Trajectories of the regret of BO versus the number of FEs during the BO process of applying EI on Levy ($n \in \{5, 10\}$) and Schwefel ($n \in \{2, 5, 10\}$). The results of the first column, second column, and third column are obtained by using different settings of the termination threshold suggested in Section 3.2 of the main paper respectively.

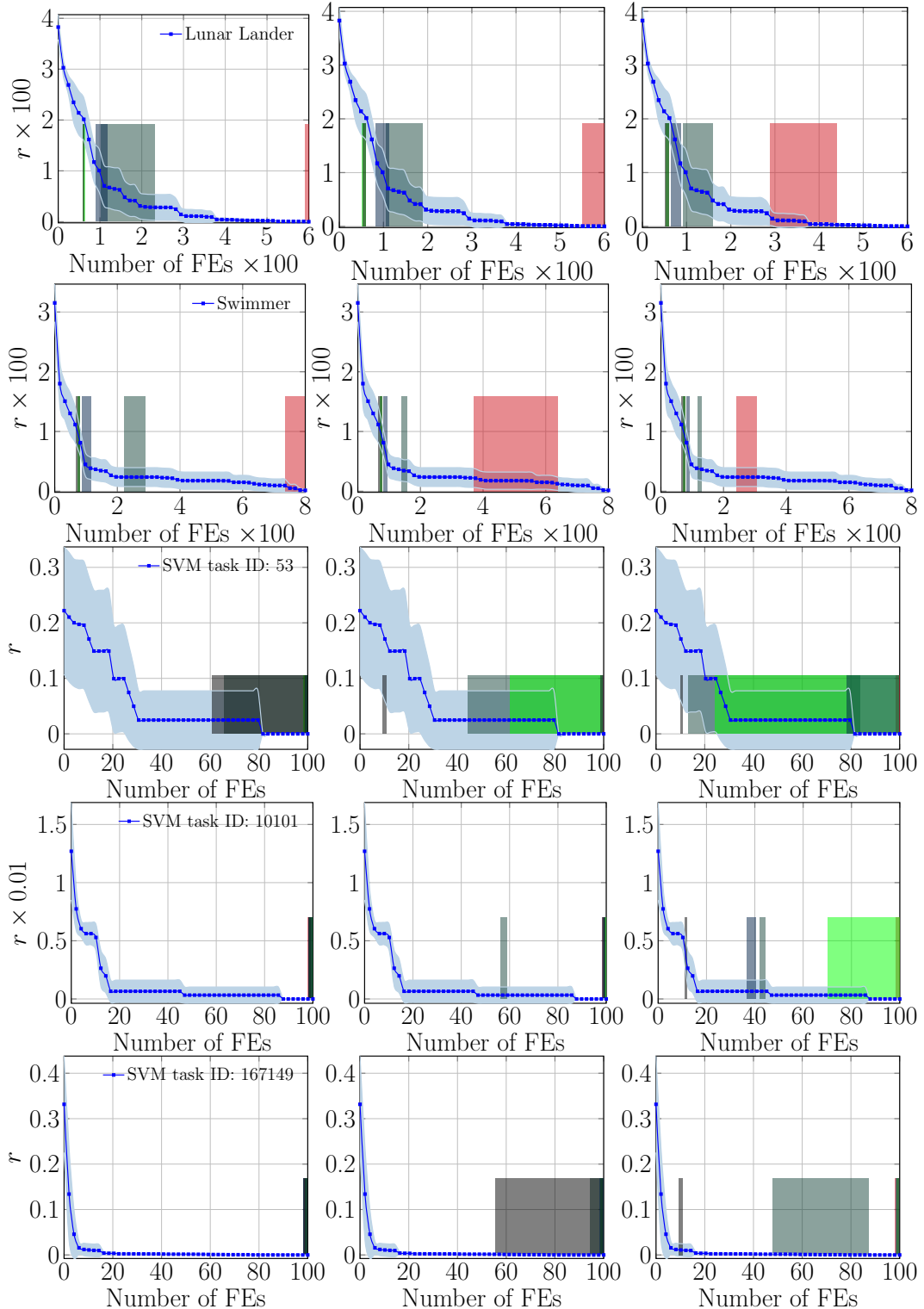


Figure 37: Trajectories of the regret of BO versus the number of FEs during the BO process of applying EI on Lunar Lander, Swimmer, and SVM (task ID: {53, 10101, 167149}). The results of the first column, second column, and third column are obtained by using different settings of the termination threshold suggested in Section 3.2 of the main paper respectively.

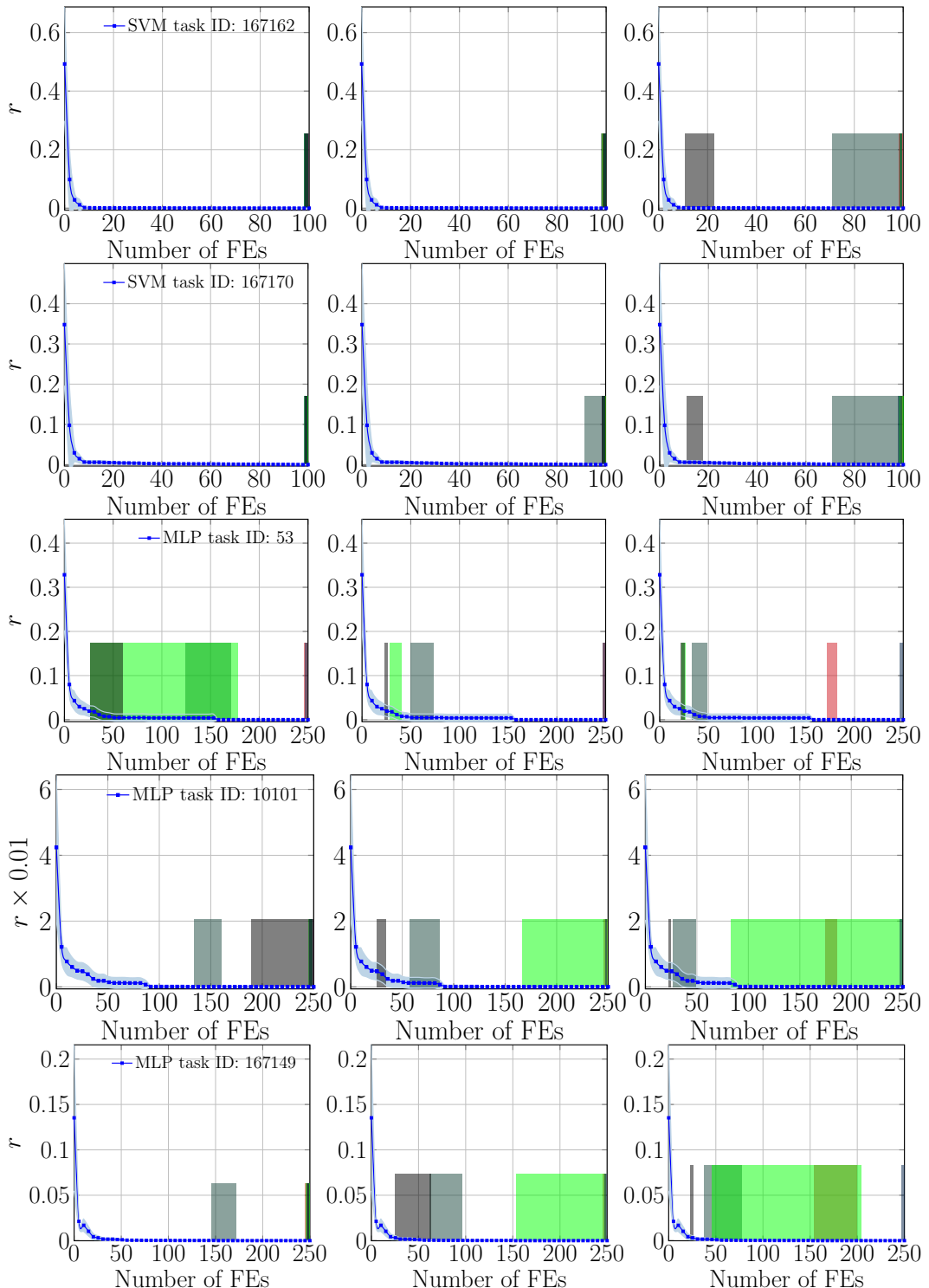


Figure 38: Trajectories of the regret of BO versus the number of FEs during the BO process of applying EI on SVM (task ID: {167162, 167170}) and MLP (task ID: {53, 10101, 167149}). The results of the first column, second column, and third column are obtained by using different settings of the termination threshold suggested in Section 3.2 of the main paper respectively.

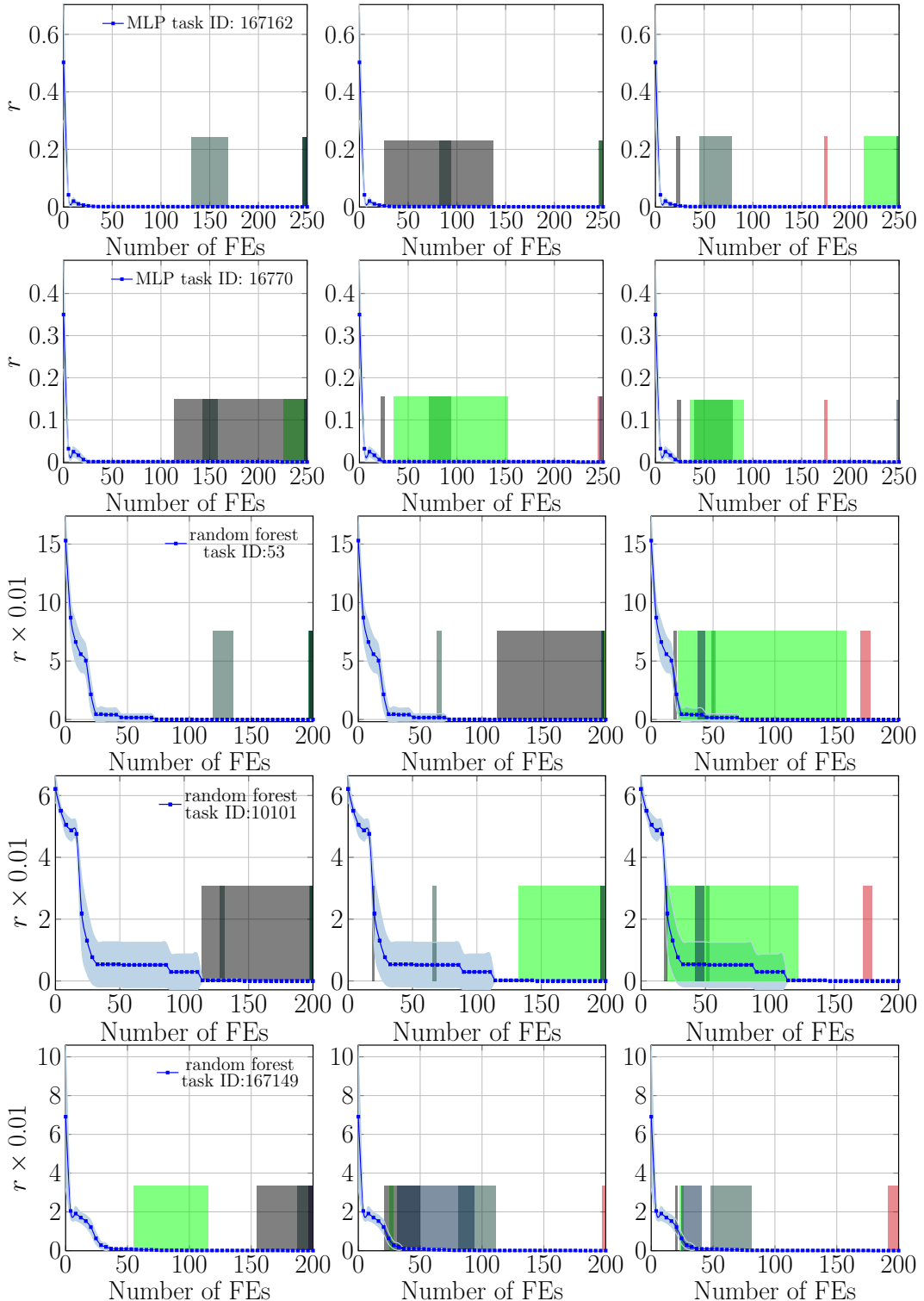


Figure 39: Trajectories of the regret of BO versus the number of FEs during the BO process of applying EI on MLP (task ID: {167162, 167170}) and random forest (task ID: {53, 10101, 167149}). The results of the first column, second column, and third column are obtained by using different settings of the termination threshold suggested in Section 3.2 of the main paper respectively.

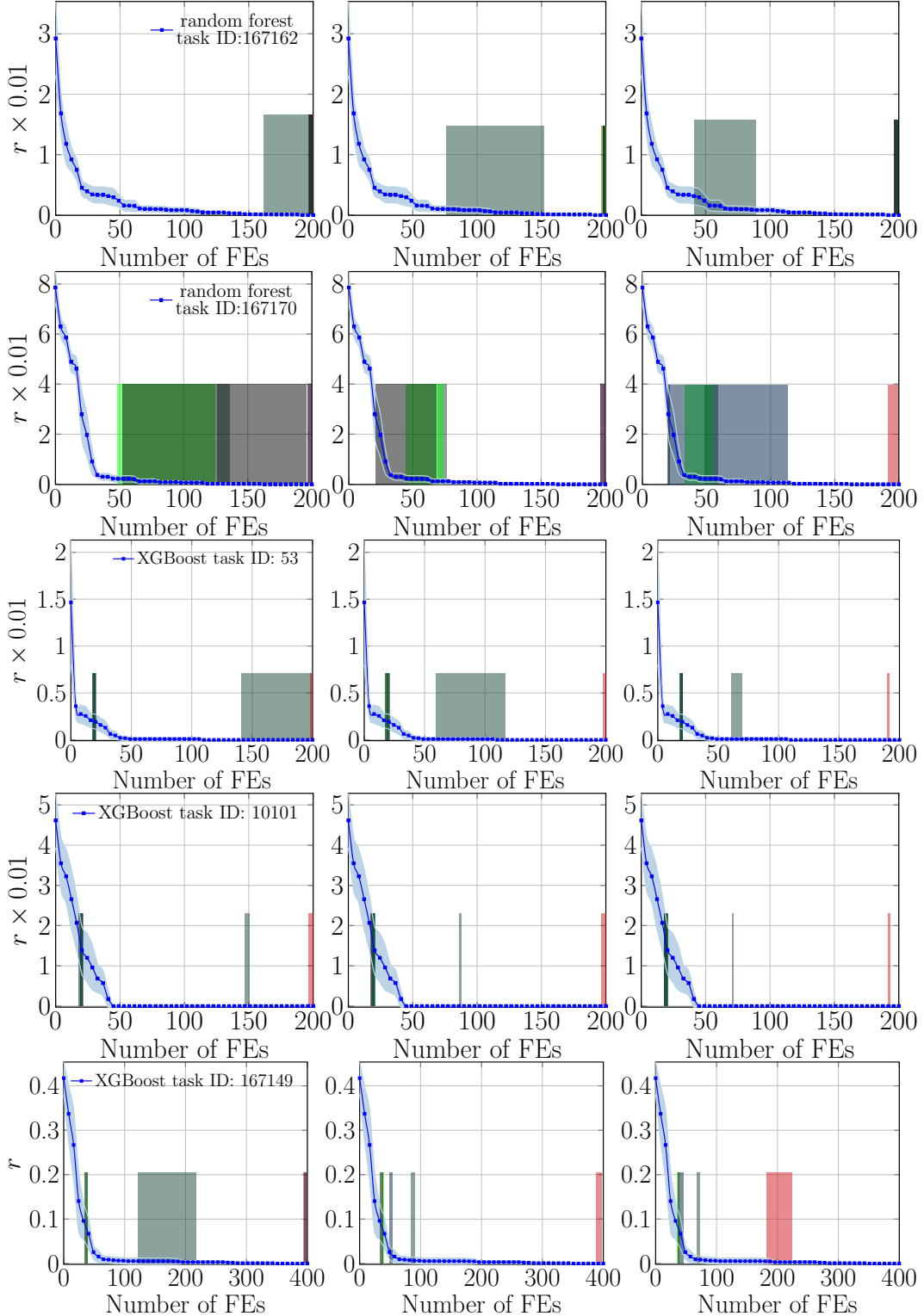


Figure 40: Trajectories of the regret of BO versus the number of FEs during the BO process of applying EI on random forest (task ID: {167162, 167170}) and XGBoost (task ID: {53, 10101, 167149}). The results of the first column, second column, and third column are obtained by using different settings of the termination threshold suggested in Section 3.2 of the main paper respectively.

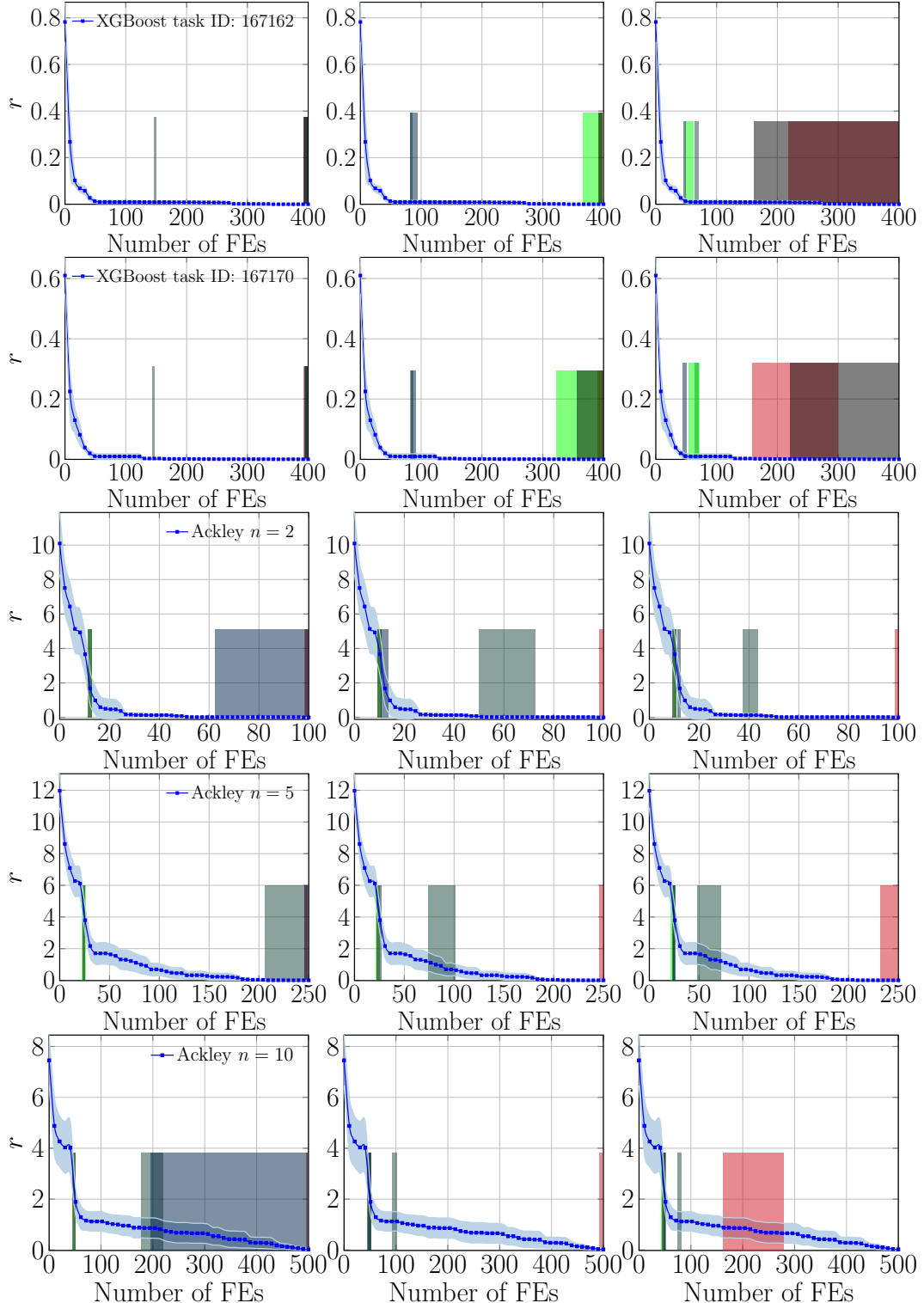


Figure 41: Trajectories of the regret of BO versus the number of FEs during the BO process of applying EI on XGBoost (task ID: $\{167162, 167170\}$), and applying PI on Ackley ($n \in \{2, 5, 10\}$). The results of the first column, second column, and third column are obtained by using different settings of the termination threshold suggested in Section 3.2 of the main paper respectively.

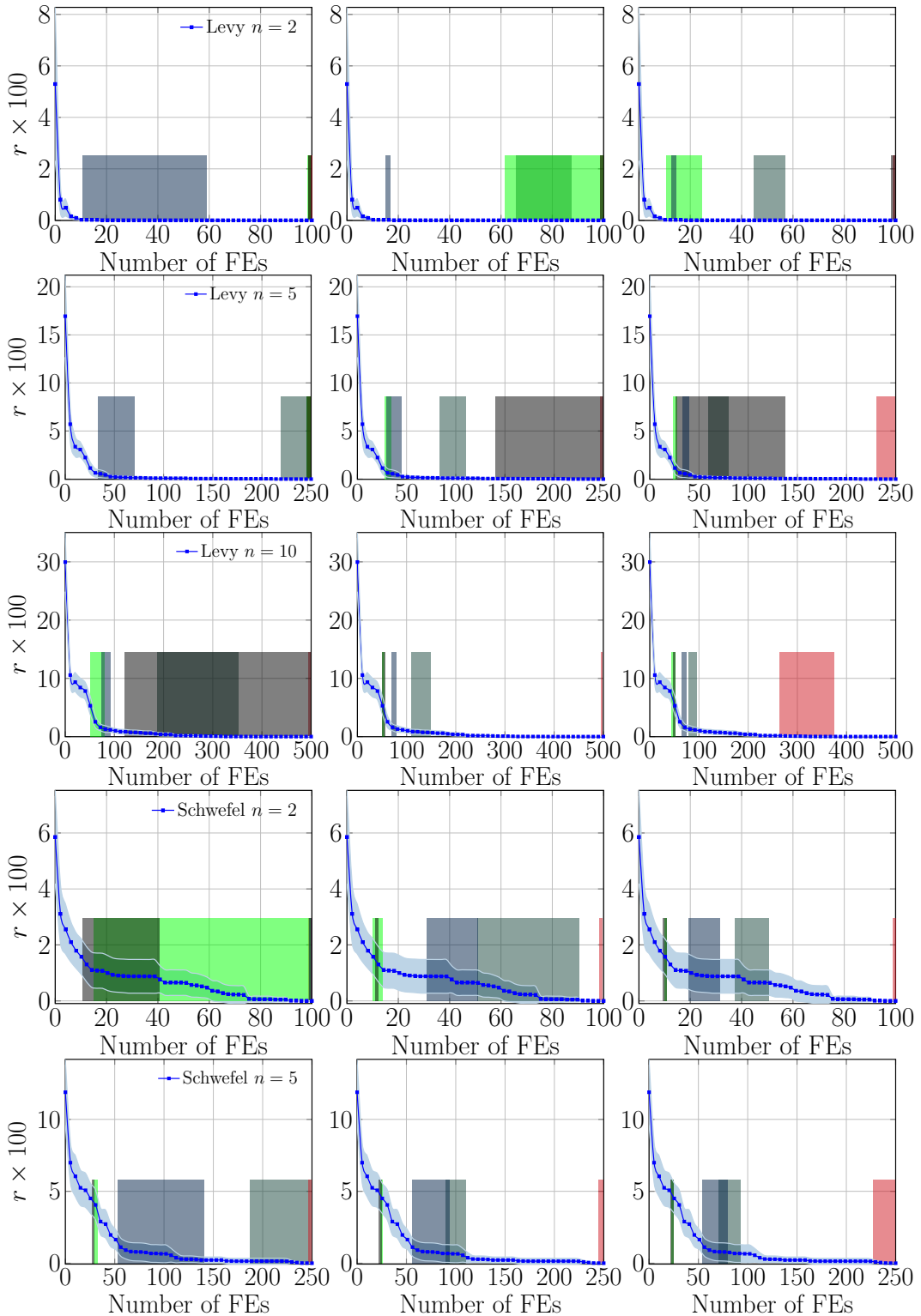


Figure 42: Trajectories of the regret of BO versus the number of FEs during the BO process of applying PI on Levy ($n \in \{2, 5, 10\}$) and Schwefel ($n \in \{2, 5\}$). The results of the first column, second column, and third column are obtained by using different settings of the termination threshold suggested in Section 3.2 of the main paper respectively.

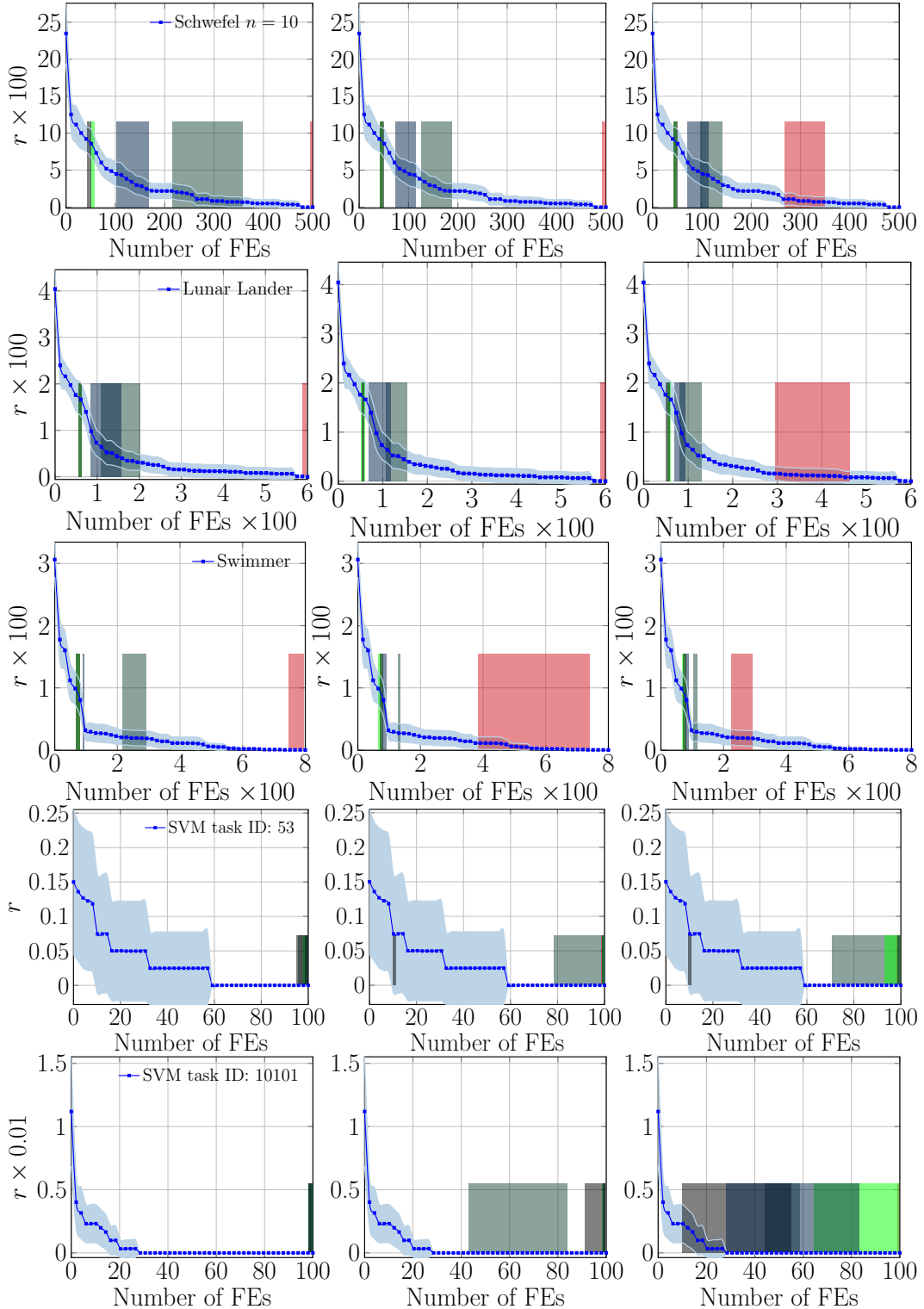


Figure 43: Trajectories of the regret of BO versus the number of FEs during the BO process of applying PI on Schwefel ($n = 10$ }), Lunar Lander, Swimmer and SVM (task ID: {53, 10101}). The results of the first column, second column, and third column are obtained by using different settings of the termination threshold suggested in Section 3.2 of the main paper respectively.

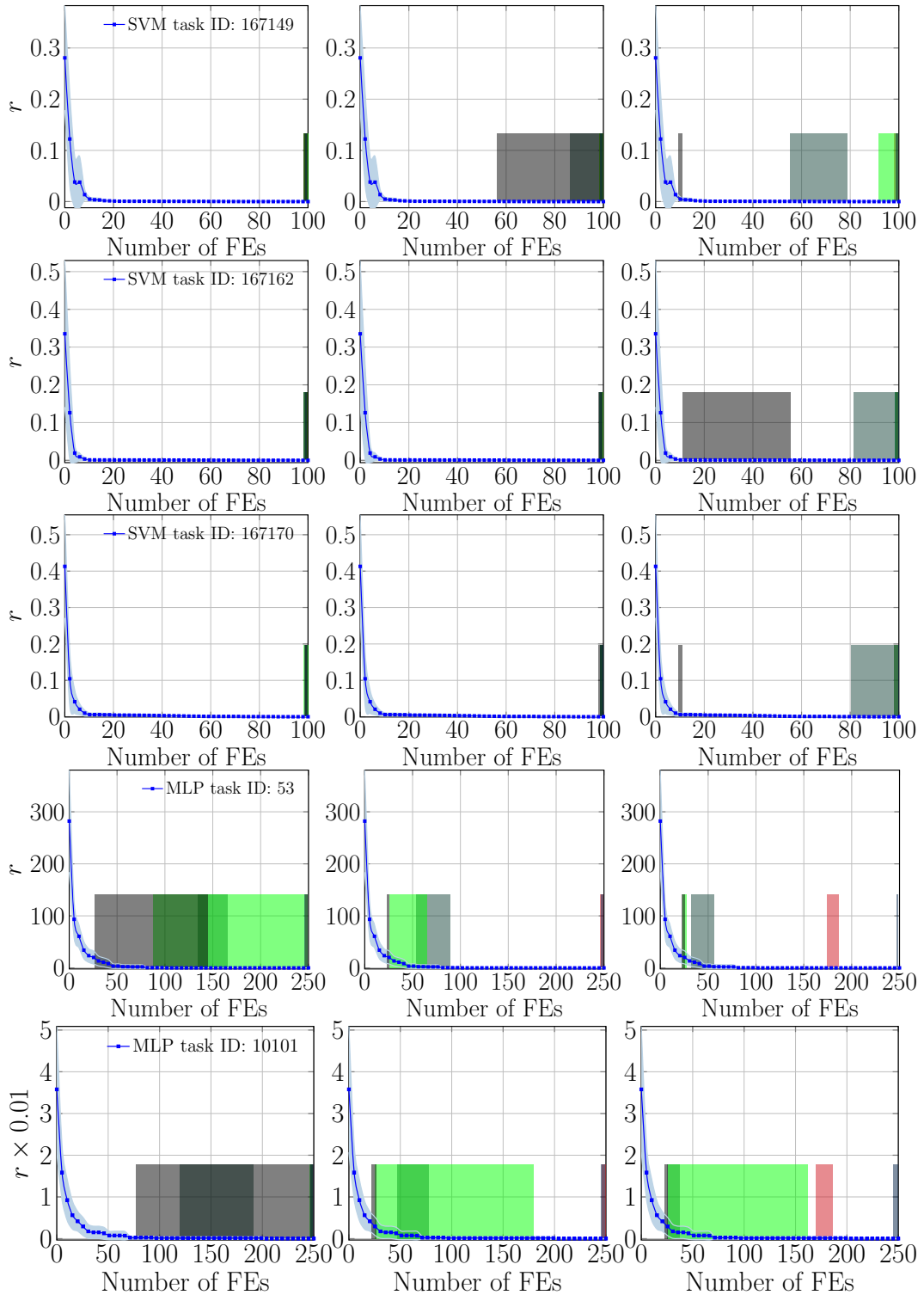


Figure 44: Trajectories of the regret of BO versus the number of FEs during the BO process of applying PI on SVM (task ID: {167149, 167162, 167170}) and MLP (task ID: {53, 10101}). The results of the first column, second column, and third column are obtained by using different settings of the termination threshold suggested in Section 3.2 of the main paper respectively.

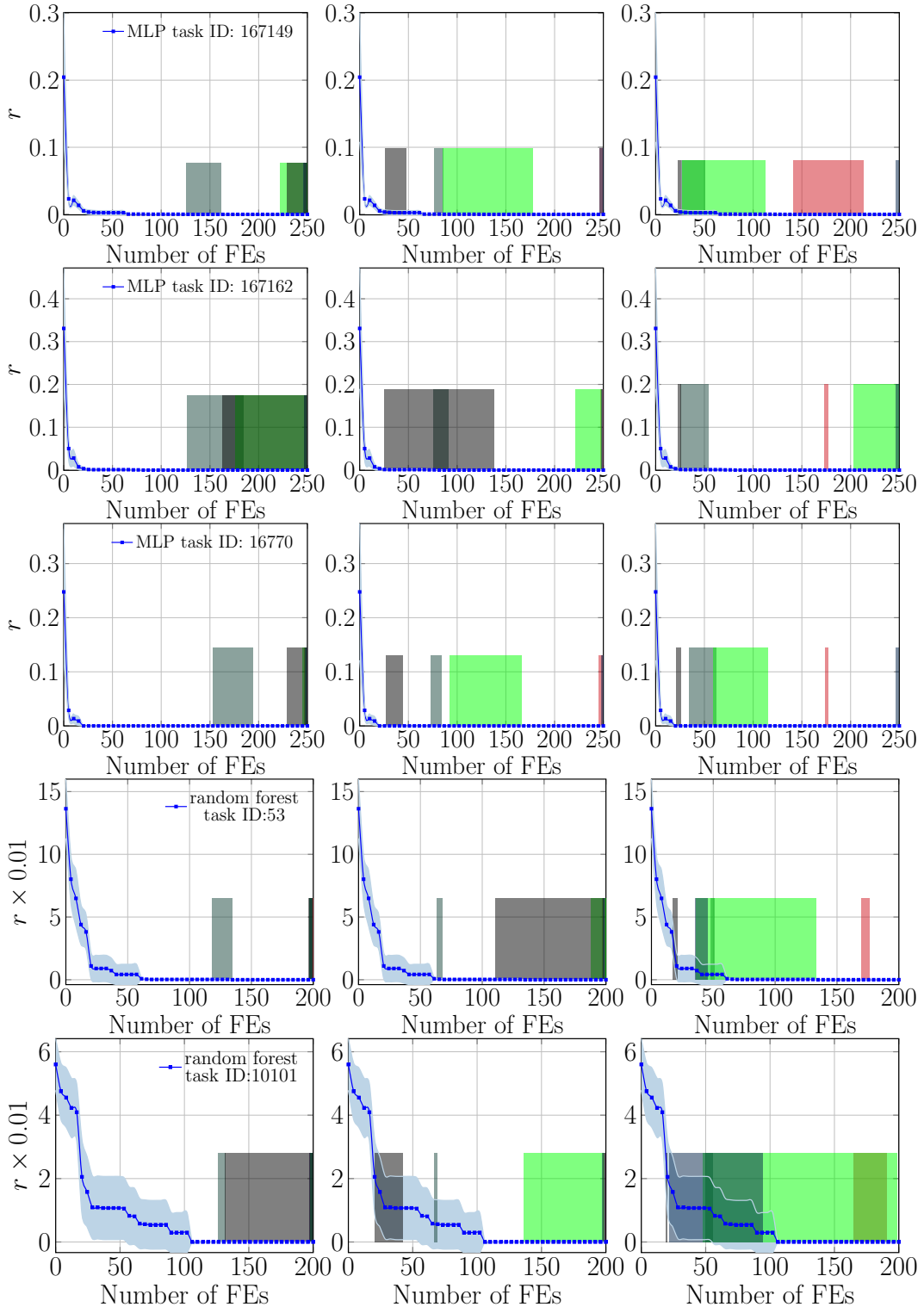


Figure 45: Trajectories of the regret of BO versus the number of FEs during the BO process of applying PI on MLP (task ID: {167149, 167162, 167170}) and random forest (task ID: {53, 10101}). The results of the first column, second column, and third column are obtained by using different settings of the termination threshold suggested in Section 3.2 of the main paper respectively.

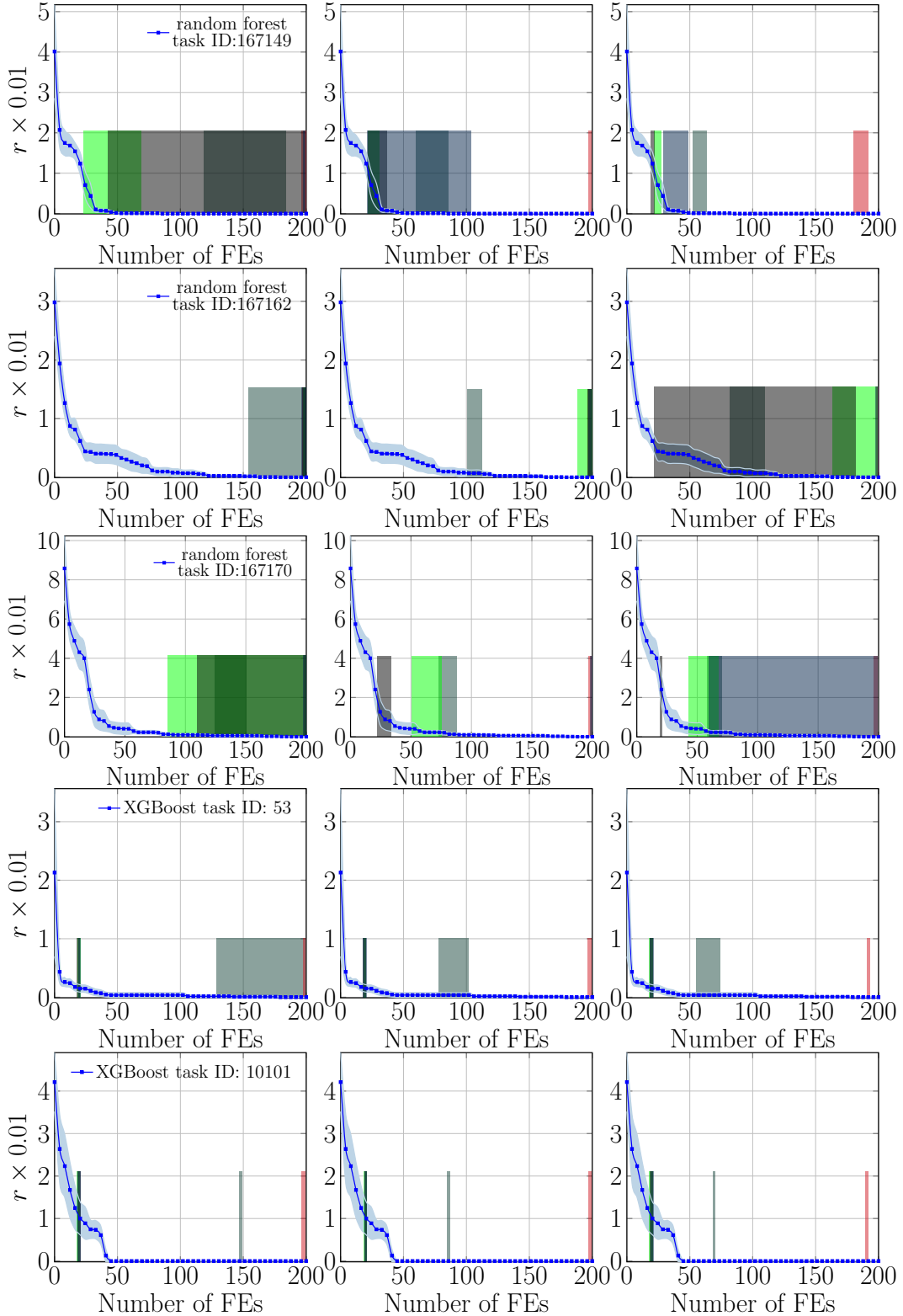


Figure 46: Trajectories of the regret of BO versus the number of FEs during the BO process of applying PI on random forest (task ID: {167149, 167162, 167170}) and XGBoost (task ID: {53, 10101}). The results of the first column, second column, and third column are obtained by using different settings of the termination threshold suggested in Section 3.2 of the main paper respectively.

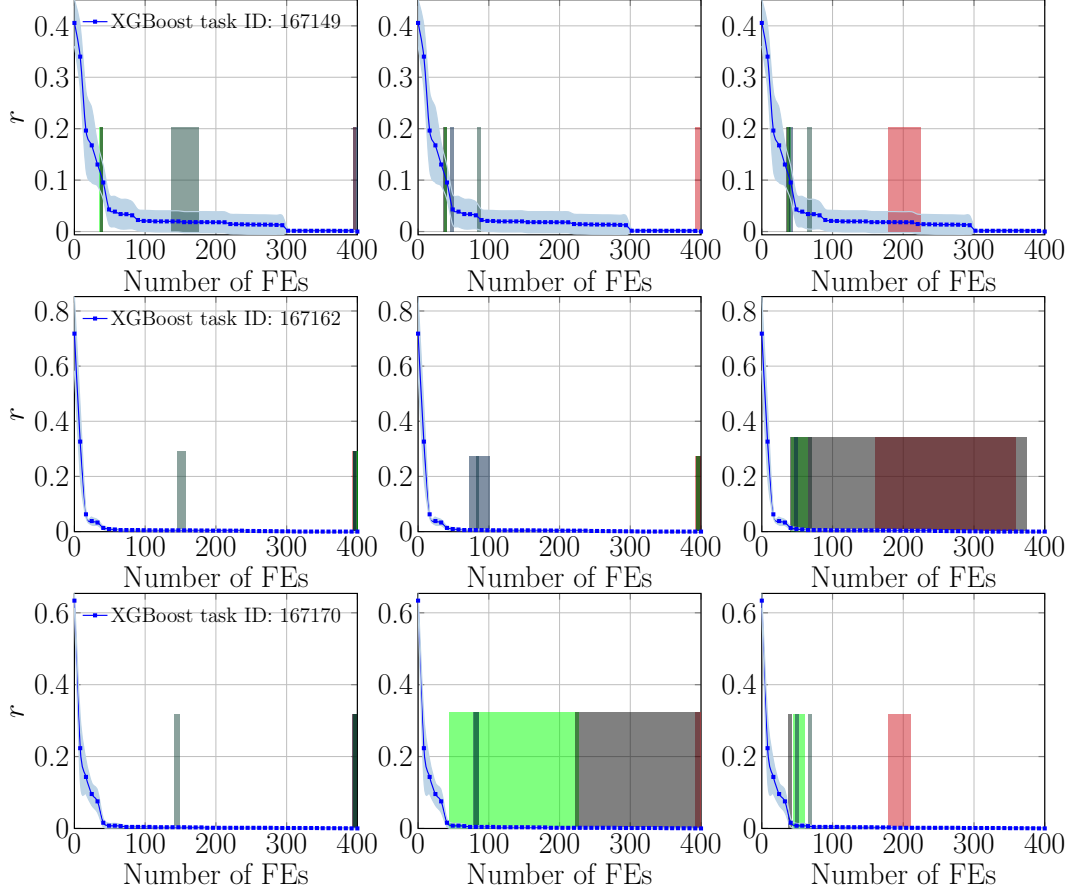


Figure 47: Trajectories of the regret of BO versus the number of FEs during the BO process of applying PI on XGBoost (task ID: {167149, 167162, 167170}). The results of the first column, second column, and third column are obtained by using different settings of the termination threshold suggested in Section 3.2 of the main paper respectively.